# Phago-mixotrophy of small eukaryotic phytoplankton might alleviate iron limitation in HNLC Southern Ocean

Denise Rui Ying Ong [1,*], Andrés Gutiérrez-Rodríguez [2,3], Karl A. Safi [4], Dominique Marie [5], Karen E. Selph [6], Michael R. Stukel [7,8], Moira Décima [2,9], Adriana Lopes dos Santos [1,10]

[1] Asian School of the Environment, Nanyang Technological University, Singapore

[2] National Institute of Water and Atmospheric Research, Wellington, New Zealand

[3] Instituto Español de Oceanografía, Centro Oceanográfico de Gijón, Avda. Príncipe de Asturias 70 BIS, 33212, Gijón, Spain

[4] National Institute of Water and Atmospheric Research, Hamilton 3216, New Zealand

[5] Sorbonne Université, CNRS, UMR7144, Team ECOMAP, Station Biologique de Roscoff, Roscoff, 29680, France

[6] Department of Oceanography, University of Hawaii at Mnoa, Honolulu, HI, 96822, USA

[7] Department of Earth, Ocean and Atmospheric Science, Florida State University, Tallahassee, FL, USA

[8] Center for Ocean-Atmospheric Prediction Studies, Florida State University, Tallahassee, FL, USA

[9] Scripps Institution of Oceanography, University of California at San Diego, San Diego, CA 92093, USA

[10] Department of Biosciences, University of Oslo, PO Box 1066 Blindern, 0316, Oslo, Norway

[*] Corresponding author: denise.ry.ong@gmail.com

**ORCID**

- Denise Rui Ying Ong: 0000-0001-6053-6948
- Adriana Lopes dos Santos: 0000-0002-0736-4937
- Andrés Gutiérrez-Rodríguez: 0000-0003-1274-3752
- Karl A. Safi: 0000-0002-7785-1909
- Karen E. Selph: 0000-0001-7281-4706
- Michael R. Stukel: 0000-0002-7696-6739
- Moira Décima: 0000-0003-0340-648X

Date: January 8, 2024

# Abstract

Small phytoplankton, consisting of pico and nano size fractions, are diverse in size and taxonomy. Yet, the differences in their productivity and taxonomic diversity are poorly described. Here, we measured the cell-specific carbon fixation rates of small phytoplankton (picocyanobacteria *Synechococcus*, picoeukaryotes and nanoeukaryotes) populations and unveiled their associated community composition in oligotrophic subtropical (ST) and high-nutrient low-chlorophyll (HNLC) subantarctic (SA) waters. We coupled 24 h *in situ* radiolabelled $^{14}$C incubations to flow cytometry sorting (FCM-sorting) and DNA metabarcoding from the same incubated samples, offering a direct account of the community associated with the carbon fixation rates measured. In both water masses, nanoeukaryotes had the highest cell-specific carbon fixation rate, followed by picoeukaryotes and *Synechococcus* (2.24 ś 29.99, 2.18 ś 2.08 and 0.78 ś 0.55 fgC cell$^{-1}$ h$^{-1}$, respectively). The cell-specific carbon fixation rates and growth rates of *Synechococcus* were 3-fold higher in ST compared to SA waters, while the rates of picoeukaryotes and nanoeukaryotes had no significant difference between the biogeochemically contrasting water masses. Despite distinct community composition between picoeukaryote and nanoeukaryote populations, the FCM-sorted picoeukaryote community in SA waters and the nanoeukaryotic community in both ST and SA waters were dominated by taxa with reported phago-mixotrophic strategies (Chrysophyceae, Dinophyceae and Prymnesiophyceae), suggesting phago-mixotrophy might alleviate nutrient stress in iron limited conditions for discrete small photosynthetic eukaryote populations.


**Keywords**: cell-specific carbon fixation rates, phago-mixotrophy, Southern Ocean, small marine phytoplankton, metabarcoding

# Introduction

Marine phytoplankton accounts for half of the Earth's primary production (Field et al. 1998), and 10-20% of which is exported into the deep ocean through the biological carbon pump (De La Rocha and Passow 2014; Falkowski et al. 1998). This process represents the only true net sink for anthropogenic carbon dioxide over the past 200 years (Sabine et al. 2004). In the open ocean where low nutrient concentrations prevails, small phytoplankton, which include pico (0.2 to 2–3 $\mu$m, Vaulot et al. 2008) and nano (2–3 to 20 $\mu$m) size cells, are dominant as their lower diffusion boundary layers and higher surface to volume ratio allows a more efficient nutrient acquisition compared to larger phytoplankton hein1995.

Small phytoplankton populations distinguished by size (pico and nano) and taxonomic domains (cyanobacteria and eukaryotes) can exhibit a wide range of primary production rates (C $m^{-3}$ $day^{-1}$) due to marked differences in cell abundance or biomass, as well as carbon fixation or growth rates. Differences in primary production between pico and nanophytoplankton have been quantified by combining radiolabelled $^{14}C$ or stable isotope $^{13}C$ incubation experiments with size fractionated measurements of the community. Such experiments have shown high contributions of small phytoplankton to primary production (50–80%) in low nutrient conditions (Garcia et al. 2007; Larsson and Hagström 1982; McKay et al. 2005).

Flow cytometry sorting (FCM-sorting) can be used to separate the phytoplankton community by cell size (pico and nano), and further divided by taxonomic domains based on fluorescence of natural photosynthetic pigments such as phycoerythrin (e.g., cyanobacteria and cryptophytes) and chlorophyll *a* (e.g., other photosynthetic eukaryotes) (Marie et al. 2010). The rate of carbon fixation per cell (C $cell^{-1}$ $h^{-1}$) by the uptake of isotopic tracers of a given phytoplanktonic population can be then achieved through direct liquid scintillation counting (cell-specific) of the FCM-sorted population (Jardillier et al. 2010; Li 1994; Rii et al. 2016b) or more recently (and yet less accessible) at the single-cell level by nanoscale secondary ion mass spectrometry (nanoSIMS) (Berthelot et al. 2019; Duerschlag et al. 2021; Irion et al. 2021). These approaches have shown that photosynthetic picoeukaryotes' contribution to picophytoplankton productivity (also measured as C $m^{-3}$ $day^{-1}$) can be similar or higher than the more abundant picocyanobacteria populations, as photosynthetic picoeukaryotes are larger and have higher growth rates (Jardillier et al. 2010; Li 1994; Rii et al. 2016b). Furthermore, within small eukaryotes, larger cells have higher rates of carbon fixation per cell compared to smaller cells (<2 µm), which results in similar or higher productivity (Duhamel et al. 2019; Irion et al. 2021; Jardillier et al. 2010; Zubkov 2014).

In addition to size, taxonomic affiliation and diversity within picocyanobacteria and small photosynthetic eukaryotes can also contribute to the carbon fixation rate variability of these groups. Traits such as cell size, morphology, nutrient requirements and acquisition, and trophic activity (e.g., autotrophy vs. mixotrophy) differ in their conservatism within and between taxonomic lineages (Cavender-Bares et al. 2009; Litchman et al. 2010). Only a few studies using cell-specific or single-cell (nanoSIMS) approaches have characterised the taxonomic composition of the target phytoplanktonic community by DNA-based methods, including fluorescence *in situ* hybridisation (FISH) (Grob et al. 2011; Hartmann et al. 2014; Jardillier et al. 2010) and DNA sequencing of marker genes either on the total community (Duerschlag et al. 2021; Irion et al. 2021) or specifically on FCM-sorted populations (Duhamel et al. 2019; Rii et al. 2016b). Despite differences in productivity (Irion et al. 2021; Rii et al. 2016b), and evidence of phylogeography (Farrant et al. 2016; Logares et al. 2020), as well as differences in community composition between pico and nanoeukaryote assemblages (Obiol et al. 2020; Sommer et al. 2017), there is still limited information on the influence of taxonomic diversity on productivity of distinct small phytoplankton populations (Duhamel et al. 2019; Irion et al. 2021; Rii et al. 2016b). Direct measurements of small phytoplankton cell-specific carbon fixation rates has mostly been conducted in tropical and subtropical latitudes (Duerschlag et al. 2021; Grob et al. 2011; Jardillier et al. 2010; Rii et al. 2016b), with only one study conducted in the Southern Ocean (Irion et al. 2021).

The Southern Ocean accounts for a significant proportion of total phytoplankton net primary productivity and carbon export, comprising almost half of the total anthropogenic carbon dioxide uptake by the ocean (Frölicher et al. 2015). The region is dominated by high-nutrient, low-chlorophyll (HNLC) conditions, representing the largest zone globally where primary production is limited by low iron concentrations (Boyd et al. 2000; de Baar et al. 1995), with a growing appreciation for the importance of small phytoplankton in production and export (Flynn et al. 2023; Irion et al. 2021). Our study was conducted across the southern subtropical frontal zone (STFZ) that extends to the east of Aotearoa-New Zealand in the southwest Pacific Ocean, separating biogeochemically contrasting subtropical (ST) and subantarctic (SA) water masses (Chiswell et al. 2015; Sutton 2001). ST waters to the north are warm and mainly nitrogen limited (Chiswell et al. 2022; Hall et al. 1999; Zentara and Kamykowski 1981), while SA waters to the south are considered HNLC, where low iron is the primary limiting factor for phytoplankton growth and production (Boyd et al. 1999; Boyd et al. 2010; Dugdale et al. 1995).

In this study, we took advantage of the strong physico-chemical and productivity gradients characteristic of the STFZ (Chiswell et al. 2022; Nodder et al. 2007) to assess the relationship between productivity and diversity of small phytoplankton populations in contrasting ST and HNLC SA wa-

ters. We measured cell-specific carbon fixation rates and characterised the taxonomic composition of three small marine phytoplankton populations (picocyanobacteria *Synechococcus*, picoeukaryotes and nanoeukaryotes) by 24-h *in situ* radiolabelled $^{14}C$ incubations coupled to FCM-sorting during the austral spring productive season. The $^{14}C$-uptake rates and taxonomic composition by DNA metabarcoding were obtained on sorted populations which originated from the same incubated samples, providing a direct account of the community associated with the carbon fixation rates. To our knowledge, this is the first study that has applied such methodology. By conducting such experiments and measurements across biogeochemically contrasting ST and SA water masses, we aimed to better understand the relationship between small phytoplankton diversity and productivity.

# Material and Methods

## Study area and sampling

Sampling was carried out during the Salp Particle expOrt and Oceanic Production (SalpPOOP) cruise on board the R/V Tangaroa (TAN1810, 21st October 21st November 2018), near the Chatham Rise, east of Aotearoa-New Zealand. The sampling strategy was designed based on Lagrangian experiments (hereafter referred to as cycles), following the same water parcel (Figure 1A). A satellite-tracked floating array with a drogue centred at 15 m depth allowed us to follow the same water parcel for repeated water column measurements and *in situ* incubations in the euphotic zone over multiple days (Landry et al. 2009). Water parcels were identified based on physical (temperature and salinity) measurements, while nutrient measurements confirmed the expected biogeochemical differences between these water masses (Décima et al. 2023). Profiles of temperature, salinity, fluorescence and photosynthetically active radiation (PAR) from the water column were obtained with a Seabird (SBE 911plus) CTD (Conductivity-Temperature-Depth) attached to a rosette frame with 10 L Niskin bottles for water collection. Each experimental cycle was sampled for periods of 3 to 5.5 days, with two in subtropical waters (ST1 and ST2) and three in subantarctic waters (SA-Sc, SA1 and SA2) (Figure 1A). SA-Sc lasted for 7.5 days and the cycle was after divided into two periods of 5 (A) and 2.5 days (B) based on differences of nutrient regime, phytoplankton biomass and productivity (Décima et al. 2023). The data of this work only includes those obtained in period A. Water samples were obtained from daily pre-dawn CTDs (0200 deployment) to 1) conduct $^{14}$C-uptake experiments, 2) obtain phytoplankton cell abundances by flow cytometry and 3) determine total community taxonomic composition by DNA sequencing. Morning CTDs (0900-1200h deployment) were obtained from several depths (Table S1) to measure nutrient and size-fractionated Chlorophyll *a* (Chl *a*) concentration as described in Décima et al. (2023) (see Supplementary Material).

## Primary production experiments

Small phytoplankton cell-specific carbon fixation rates and volumetric net primary production (NPP) rates were measured by $^{14}$C-uptake during 24-h *in situ* incubation experiments (Peterson 1980). Cell-specific experiments were conducted in the surface mixed layer (12 m) and the deep chlorophyll maximum (DCM, from 25 to 70 m), while standard volumetric NPP experiments were carried out at 6 depths, from 5 m to below the DCM (from 50 to 100 m), with specific depths of each cycle presented in Table S1. Cell-specific and volumetric NPP experiments were conducted between one and

four times in each experimental cycle, yielding a total of 11 and 17 incubation profiles, respectively. For cell-specific carbon fixation rate measurements, 7.4 × $10^6$ (200 µCi) was added to 36 mL of seawater in a 50 mL falcon tube using a 5 mCi 14C-sodium bicarbonate stock solution (Perkin Elmer, NEC086H005MC). After gently homogenization of the spiked sample, 100 µL controls were taken on ethanolamine to quantify initial radioactivity added. The remaining seawater was distributed into four gas tight HPLC glass vials (8 mL; 3 light + 1 dark control) to a total volume of 7.4 mL. The four vials (3 light + 1 dark control) from each depth were placed in 320 mL PC clear bottles filled with seawater from the same depth of experiment water collection to avoid temperature variation. Two sets of duplicates of 1.5 mL seawater were taken from each radiolabelled vial after incubation. Set 1 ($^{14}$C-uptake measurements) was preserved with a solution of 25% glutaraldehyde and 1/10 pluronic acid mix at 1% final concentration, incubated at room temperature for 15 minutes, followed by flash-freezing in liquid nitrogen. Set 2 (DNA sequencing) was preserved with a solution of DMSO and 1/100 pluronic acid mix at 10% final concentration, incubated at room temperature for 10 minutes and flash-frozen in liquid nitrogen. All samples were stored at -80 °C until fluorescence-activated cell sorting by flow cytometry.

Volumetric NPP experiments with standard volume incubations (320 mL) were conducted as described in Décima et al. (2023). To evaluate the impact of a smaller volume incubation used for cell-specific measurements, small volume incubations (7.4 mL) for NPP measurements at surface and DCM depths were also obtained as described in the Supplementary Material.

## Flow cytometry

Samples preserved in glutaraldehyde ($^{14}$C-uptake measurements) or DMSO (DNA sequencing) from cell-specific incubations were sorted using FACSAria flow cytometer (Becton Dickinson, San Jose, CA) (see Supplementary Material). Cells for $^{14}$C-bicarbonate incorporation measurements and DNA sequencing were sorted in purity mode and collected into Eppendorf tubes containing ethanolamine and Tris-EDTA lysis buffer (Tris 10 mM, EDTA 1 mM, and 1.2% Triton, final concentration) (Gérikas Ribeiro et al. 2018), respectively (Tables S2 and S3). Additional aliquots of seawater taken from the same CTD casts used for cell-specific rate incubations were 1) preserved in paraformaldehyde (0.5% final concentration) for later shore-based analyses on a CytoFlex S flow cytometer (Beckman Coulter) after staining with Hoechst 34580 (Selph 2021), for *Synechococcus* enumeration, and 2) analysed within 1-2 h, unpreserved, for phytoplankton cell enumeration (only eukaryotes) and forward scatter (FSC) signals (all populations) using a shipboard Accuri C6 Plus flow cytometer (Becton-Dickinson), with

populations identified based on the Chl *a* fluorescence signal as described in Stukel et al. (2021).

## $^{14}$C-fixation rates

The radioactivity retained in cells from FCM-sorting and harvested on the filters, for cell-specific and volumetric NPP measurements respectively, were measured as disintegrations per minute (DPM) using a Beckman Liquid Scintillation counter following procedures as described in Gutiérrez-Rodríguez et al. (2020). DPM from dark incubation was subtracted from light incubation to account for the light independent stage of carbon fixation. DPM for volumetric NPP was converted to mmolC m$^{-3}$ day$^{-1}$ using volume, total added activity and measured dissolved inorganic carbon concentrations (Duhamel and Moutin 2009). The volumetric NPP rates were integrated across the six depths using a trapezoidal integration.

To obtain cell-specific carbon fixation rates of different groups, three quantities of 2000, 4000 and 10000 cells belonging to *Synechococcus* and picoeukaryotes populations were sorted from each vial, using the protocol described above, to quantify the total DPM (Table S2). DPM per cell was then calculated using type I linear regression. For nanoeukaryotes, 1000 cells from each vial were sorted and filtered, after which the total DPM was divided by 1000 to calculate DPM per cell for each vial. DPM per cell from dark vials were subtracted from light vials. Cell-specific carbon fixation rates (fgC cell$^{-1}$ h$^{-1}$) were calculated based on DPM per cell as follows:

$$\text{Cell-specific } CO_2 \text{ fixation} = DIC \times \frac{DPMcell}{SA \times 24} \times 1.05 \times 10^9$$

where DIC = dissolved inorganic carbon (mgC L$^{-1}$), DPMcell = DPM per cell after incubation for 24 h as calculated from above, SA = standard activity in 1 mL (DPM per mL). 24 is used to convert units from day$^{-1}$ to h$^{-1}$, 1.05 is used to account for the differential uptake between $^{14}$C and $^{12}$C, and $10^9$ is used to convert between units from L to m$^3$ and from mg to fg.

We excluded measurements from experiment 7 in ST1 from the analysis due to uncertainty in the values of DPM. Raw measurements are reported in the Supplementary Material (Figures S1, S2, S3 and S4).

Group-specific productivity (mgC m$^{-3}$ day$^{-1}$) was calculated by multiplying cell-specific carbon fixation rates with cell abundance measured by FCM in seawater samples from the same CTD cast and depth used for $^{14}$C-bicarbonate incubation (Figure S1). There were no cell abundance measurements at the surface (12 m) of SA1 experiment 5 (station 176), therefore the average cell abundance at the surface

of cycle SA1 was used instead.

## Growth rates

To derive growth rates from cell-specific carbon fixation rates, we first estimated cell diameter (µm) and subsequently cell biovolume (BV; µm$^3$), assuming spherical shape, of unpreserved *Synechococcus*, photosynthetic picoeukaryotes and nanoeukaryotes from average FSC cytometric signal at each corresponding incubation and depth, normalised to polystyrene reference beads (Polysciences, Inc., Warrington, PA). Average carbon biomass per cell (C; pgC cell$^{-1}$) of each photosynthetic population was calculated based on BV using the conversion factor of $C = BV \times 0.265$ pgC µm$^{-3}$ for *Synechococcus* (Bertilsson et al. 2003), and $C = 0.216 \times BV^{0.939}$ for eukaryotic cells (Menden-Deuer and Lessard 2000).

There were no FSC measurements of SA1 in experiment 5 (station 176) and experiment 6 (station 188), therefore the average cell biomass at each depth of cycle SA1 was used instead. Growth rate (day$^{-1}$) was calculated for each vial from the $^{14}$C-bicarbonate incubation:

$$\text{Growth rate (day}^{-1}) = \frac{\text{Cell-specific } CO_2 \text{ fixation (pg cell}^{-1}\text{ h}^{-1})}{\text{Carbon biomass per cell (pg cell}^{-1})} \times 24$$

## DNA extraction, PCR and amplicon analysis

Seawater volumes of 1.42.4 L were filtered through a 0.22 µm pore-size Sterivex filter, flash frozen in liquid nitrogen and stored at -80 °C until processed (Table S4). DNA from filtered seawater was extracted using the DNeasy mini Blood and Tissue Kit (Qiagen, Germany). DNA from the sorted cells was extracted using three cycles of flash-freezing and thawing in liquid nitrogen (Gérikas Ribeiro et al. 2018) (Table S3).

PCR was performed using the following primer sets: Nested PCR targeting *petB* gene of *Synechococcus* for filtered and sorted samples, petB-F (5'-TACGACTGGTTCCAGGAACG-3') and petB-634R (5'-GCTTVCGRATCATCARGAAG-3'), followed by petB-50F (5'-TYCAGGACATYGCTGAY-3') and petB-R (5'-GAAGTGCATGAGCATGAA-3') (Mazard et al. 2012; Ong et al. 2023); nested PCR targeting 18S rRNA (V4 hypervariable region) for sorted picoeukaryotes and nanoeukaryotes samples, 63F (5'-ACGCTTGTCTCAAAGATTA-3') and 1818R (5'-ACGGAAACCTTGTTACGA-3') (Lepere et al. 2011), followed by V4F illum (5'-CCAGCASCYGCGGTAATTCC-3') and V4R illum (5'-ACTTTCGTTCTTGATYRATGA-3') (Piredda et al. 2017); 18S rRNA seawater samples, V4F

illum and V4R illum. All first and second round PCRs were performed in duplicates and pooled together. Samples were purified, barcoded, and sequenced by the GeT-PlaGe platform of GenoToul (INRA Auzeville, France) using the Illumina MiSeq platform 2 Œ 300 bp for *petB* and 2 Œ 250 bp for 18S rRNA. Detailed protocols of PCR conditions are reported in the Supplementary Material.

Details on sequencing processing steps and taxonomic assignation can be found in the Supplementary Material. Briefly, sequence data was processed on RStudio Version 1.4.1717 (RStudio Team 2021) using DADA2 R package Version 1.12 (Callahan et al. 2016). Taxonomy was assigned against a *petB* reference sequence database (Farrant et al. 2016) reformatted for use with DADA2 (Ong et al. 2023) for *Synechococcus*, and PR2 database version 4.14 (Guillou et al. 2013) for eukaryotes. Amplicon sequence variants (ASVs) assigned to Supergroup Opisthokonta, Division Metazoa, Fungi and Pseudofungi, class Syndiniales, as well as protists assigned as heterotrophic (based on Schneider et al. 2020, full list of trophic assignment on Github) were removed and not considered in this study. Analysis was performed with *Phyloseq* R package Version 1.36.0 (McMurdie and Holmes 2013).

## Statistical analysis

We built three liner models with cell-specific carbon fixation rates, group-specific productivity or growth rates as a response variable to test for significant differences between phytoplankton group and water masses. All models were simplified by backward deletion ($P < 0.05$). The significance of fixed effects with interactions and without interactions was tested with type III and type II tests, respectively, using the *Anova* function in *car* R package (Fox and Weisberg 2019). For all models, the estimated marginal means were obtained using *emmeans* R package (Lenth 2023) and plotted to visualise differences with *ggeffects* R package (Lüdecke 2018). All estimated marginal means (EMM) with 95% CI were summarised in Table S5. Detailed descriptions of statistical analysis can be found in the Supplementary Material.

# Results

## Phytoplankton biomass, abundance, and net primary production

Two cycles were conducted in subtropical (ST) waters (ST1 and ST2) and three cycles in subantarctic (SA) waters (SA-Sc, SA1 and SA2) (Figure 1A). ST cycles were warmer (12–13 °C), more saline (34.7–35 psu) with lower nitrate, phosphate and silicic acid concentrations compared to SA cycles (10–11 °C; 34.4–34.7 psu) (Figures 1B and S5), while SA-Sc cycle showed intermediate characteristics likely reflecting the influence of the Southland Current, a coastal expression of the Subtropical Front that transport northwards a mix of neritic ST and SA waters mainly (Figure 1B and S5).

Integrated volumetric NPP for the euphotic zone was on average higher in ST than in SA cycles (mean ± SD; 603.9 ± 294.9 and 370.5 ± 194.9 mgC $m^{-2}$ $day^{-1}$, respectively), with NPP being highest in ST1 followed by coastal SA-Sc, intermediate in ST2 and lowest in oceanic SA1 and SA2 (Figure 2B). Chl *a* concentrations in the euphotic zone were on average higher in ST (58.5 ± 24.3 mg $m^{-2}$) than in SA cycles (43.6± 25.7 mg $m^{-2}$) (Figure 2A). ST1 and SA-Sc had the highest integrated Chl *a* concentration, followed by ST2 and SA1, with SA2 with the lowest concentration. Chl *a* biomass in all cycles was dominated by picoplankton (0.2–2 µm), which contributed to at least 43% of Chl *a*, followed by nanophytoplankton (2–20 µm) which accounted for 21–39% of Chl *a* (Figures 2A and S6). Microplankton (> 20 µm) had the lowest proportion of phytoplankton biomass across all the cycles (5–17%), except in SA-Sc at 30.8%.

Overall phytoplankton abundances were dominated by *Synechococcus*, followed by picoeukaryotes and nanoeukaryotes (53.7 ± 35.5, 14.6± 7 and 1.8 ± 0.7 × $10^3$ cells $mL^{-1}$, respectively) (Table 1 and Figure S5). Photosynthetic pico and nanoeukaryotes abundances were slightly higher in ST compared to SA cycles (Table 1 and Figure S5I-J) and higher at surface compared to DCM (Figure S5I-J). Conversely, *Synechococcus* abundance was higher in SA compared to ST cycles, and higher at DCM compared to surface depths (Table 1 and Figure S5H).

## Cell-specific carbon fixation rates and group-specific productivity

Cell-specific carbon fixation rates (fgC $cell^{-1}$ $h^{-1}$) and group-specific productivity (mgC $m^{-3}$ $day^{-1}$) had high variability between replicates and incubations within the same cycle, with differences of up to one order of magnitude in a few experiments (Figures S2 and S3). Despite this variability, significant differences in both measurements emerged between phytoplankton groups and water masses.

Conversely, there were no significant differences between surface and DCM for both cell-specific carbon fixation rates and group-specific productivity for any of the phytoplankton groups analysed ($P \geq 0.13$; Table S6). Therefore, the rate measurements from the two depths have been combined in the following results.

Mean carbon fixation rate was highest for nanoeukaryotes, intermediate for picoeukaryotes and lowest for *Synechococcus* (52.24 ś 29.99, 2.18 ś 2.08 and 0.78 ś 0.55 fgC cell$^{-1}$ h$^{-1}$, respectively) (Table 1). There was a significant interaction between phytoplankton group and water mass on cell-specific carbon fixation rates (ANOVA; Population × Water mass: $R^2 = 0.86$, $F_{2,115} = 5.80$, $P = 0.0004$) (Figure 3A). In ST cycles, the cell-specific carbon fixation rate of nanoeukaryotes was significantly higher than that of *Synechococcus* and picoeukaryotes ($P < 0.0001$), although differences between these picoplanktonic groups were not statistically significant ($P = 0.44$) (Figure 3A and Table S5). In SA cycles, nanoeukaryotes had the highest cell-specific carbon fixation rates, followed by picoeukaryotes and *Synechococcus*, with all three groups showing statistically significant differences ($P < 0.0001$) (Figure 3A and Table S5). The cell-specific carbon fixation rate of *Synechococcus* was three times higher in ST compared to SA cycles based on EMM ($P < 0.0001$), while there was no significant difference between the rates in ST and SA cycles for photosynthetic eukaryotes ($P > 0.37$) (Figure 3A and Table S5).

Mean group-specific productivity was highest for nanoeukaryotes, intermediate for *Synechococcus*, and lowest for picoeukaryotes (2.64 ś 2.16, 0.78 ś 0.80 and 0.65 ś 0.76 mgC m$^{-3}$ day$^{-1}$, respectively) (Table 1). Nanoeukaryotes had the highest group-specific productivity across all cycles, except in ST1, where *Synechococcus* had the highest productivity (Table 1). There was a significant difference in group-specific productivity between phytoplankton populations (ANOVA; $R^2 = 0.33$, $F_{2,\ 118} = 30.88$, $P < 0.0001$) (Figure 3B). Nanoeukaryotes showed significantly higher group-specific productivity than both *Synechococcus* and picoeukaryotes with EMM around three times higher ($P < 0.0001$), while differences were not statistically significant different between the picophytoplankton groups ($P = 0.37$) (Figure 3B and Table S5). There was no significant difference in group-specific productivity between water masses (ANOVA; $R^2 = 0.002$, $F_{1,\ 119} = 1.30$, $P = 0.26$) (Figure 3B and Table S5).

## Carbon-based growth rates and biovolume

Mean growth rate was highest for nanoeukaryotes, intermediate for picoeukaryotes and lowest for *Synechococcus* (0.29 ś 0.17, 0.24 ś 0.22 and 0.13 ś 0.09 day$^{-1}$, respectively) (Table 1 and Figure S4). There were no significant differences in growth rates between surface and DCM for any of the phy-

toplankton groups analysed ($P \geq 0.07$; Table S6). Therefore, the rate measurements from the two depths have been combined in the following results.

There was a significant interaction between phytoplankton group and water mass on growth rates (ANOVA; Population × Water mass: $R^2 = 0.86$, $F_{2,115} = 5.80$, $P = 0.0004$) (Figure 3C). In ST cycles, there was no significant difference in the growth rate between the groups ($P > 0.90$) (Figure 3C and Table S5). In SA cycles, nanoeukaryotes had the highest growth rates ($P = 0.05$), followed by picoeukaryotes and *Synechococcus* ($P = 0.001$), with all three groups showing statistically significant differences (Figure 3D and Table S5). Similar to the trends observed for cell-specific carbon fixation rates, the growth rate of *Synechococcus* was significantly higher in ST than SA cycles ($P = 0.0002$), while the growth rate of pico and nanoeukaryotes were not significantly different between the water masses ($P > 0.25$) (Table 1).

Cell diameter, and therefore cell biovolume, for each phytoplankton group was not significantly different between water mass (ST and SA cycles) and depth (surface and DCM) (Table S6). Mean cell diameter of *Synechococcus*, picoeukaryotes and nanoeukaryotes were 1.0 ± 0.05 µm, 1.2 ± 0.07 µm and 3.61 ± 0.59 µm respectively.

## Phytoplankton community composition

Within the sorted photosynthetic eukaryotic community, all alpha diversity indices of nanoeukaryotes were significantly higher than picoeukaryotes (Wilcoxon test, $P < 0.001$) (Table S7). The alpha diversity of *Synechococcus* and nanoeukaryotes were not significantly different between ST and SA cycles (unpaired t-test and Wilcoxon Rank Sum test, respectively, $P > 0.4$), while the diversity of picoeukaryotes in ST cycles was significantly lower compared to SA cycles (unpaired t-test, $P < 0.01$).

All three phytoplankton populations sorted were structured by water mass (Figure 4). Within each phytoplankton group, there were significant differences in the community composition between the ST and SA cycles (PERMANOVA-Adonis; *Synechococcus*, $R^2 = 0.18$, $P = 0.001$; picoeukaryotes, $R^2 = 0.24$, $P = 0.001$; nanoeukaryotes, $R^2 = 0.18$, $P = 0.001$). The eukaryotic phytoplankton community was also structured by size (Figure 4B), where the community composition of picoeukaryotes was significantly different from that of nanoeukaryotes (PERMANOVA-Adonis; $R^2 = 0.26$, $P = 0.001$). There were no significant differences in the community composition between surface and DCM (PERMANOVA-Adonis; *Synechococcus*, $R^2 = 0.03$, $P = 0.06$; picoeukaryotes, $R^2 = 0.02$, $P = 0.163$; nanoeukaryotes, $R^2 = 0.03$, $P = 0.07$).

The more abundant classes (represented by taxa with median relative abundance of more than 5% of

reads for any cycle) present in sorted eukaryotic pico and nanophytoplankton samples were distinct, except for Prymnesiophyceae which was present in both pico and nano size populations (Figure 5A-C). Within picoeukaryotes, Mamiellophyceae was the most abundant class contributing to 63.0% of total reads, followed by Pelagophyceae (12.4%), Prymnesiophyceae (11.0%) and Chrysophyceae (7.6%) (Figure 5A). The median relative abundance of Mamiellophyceae in ST cycles (85.8%) was twice that of oceanic SA cycles (36.6%), excluding SA-Sc where the picoeukaryotic component was nearly completely dominated by Mamiellophyceae (97.5%). The median relative abundance of Pelagophyceae and Prymnesiophyceae increased from 0% in ST cycles to 18.9% and 14.4% in SA cycles, respectively. Chrysophyceae had similar median relative abundance across ST and SA water masses (4.4% and 6.7% in ST and SA cycles, respectively). The three taxa within Mamiellophyceae, consisting of *Ostreococcus lucimarinus*, *Micromonas commoda* A2 and *Bathycococcus prasinos*, represented a large proportion of reads with each of the taxa dominating in different cycles (Figure 5B). *Ostreococcus lucimarinus* and *Micromonas commoda A2* had a higher proportion of reads in ST1, ST2 and SA-Sc, with the highest median percent of reads in SA-Sc (67.5%) and ST2 (51.7%), respectively. The median proportion of reads was lower in SA1 and SA2 for *Ostreococcus lucimarinus* (0.06%) and *Micromonas commoda* A2 (6%). *Bathycococcus prasinos* had a higher median percent of reads in ST1, SA1 and SA2 (24.7%–29.6%) compared to ST2 and SA-Sc (11.9%–13.0%). Within Prymnesiophyceae, *Phaeocystis antarctica* was identified in cycles SA1 and SA2, and dominated in SA2 with median relative abundance of 24.6% (Figure 5B).

Dinophyceae and Prymnesiophyceae were the most abundant classes within photosynthetic naneoukaryotes, accounting for 60.5% and 30.3% of reads respectively. The composition of Dinophyceae at order level changed from ST to SA cycles (Figure 5C). The proportion of unclassified Dinophyceae reads was higher in ST cycles, Peridiniales were more abundant in SA-Sc, and Gymnodiniales and Prorocentrales, of which the taxa *Karlodinium* sp. and *Prorocentrum* sp. increased in abundance in oceanic SA cycles (Figure S7). Among Prymnesiophyceae, reads assigned to Isochrysidales (comprised of only *Gephyrocapsa huxleyi*) and Prymnesiales were more common in ST cycles (median relative abundance of 8.8% and 15.7% in ST, respectively), while reads assigned to Phaeocystales was more abundant in SA cycles (median relative abundance of 17.7% in SA) (Figure 5C). *Phaeocystis antarctica* was the most abundant of the taxa within Phaeocystales, representing a median of 15.7% of reads in SA cycles, and the highest median percent of reads in SA2 (21.3%) (Figure S7). *Phaeocystis antarctica* (corresponding to the same ASV) and *Chrysochromulina* sp. (corresponding to different ASVs) were the only abundant taxa present in both pico and nanoeukaryote samples. Bacillariophyta, Cryptomonadales and Haptophyta clade HAP3 were present in lower abundance and increased in proportion in SA-Sc

(12.2%, 11.3% and 5.8% median relative abundance in SA-Sc, respectively) (Figure 5C).

Sorted *Synechococcus* was dominated by subclades Ia, Ib, IVa and IVb of clades I and IV, accounting for 99.98% of total reads (Figure 5D). Clade IV had a higher median relative abundance compared to clade I (65.8% vs 34.2%). Subclade IVa was more dominant in ST cycles (46.9%) while IVb was more dominant in SA cycles (74.4%).

To validate our approach, we compared the relative abundance of taxa (ASVs) found in the sorted populations with their relative abundance in the total community. The community composition of sorted *Synechococcus*, and picoeukaryotes and nanoeukaryotes were similar in relative abundance to filtered seawater samples (Tables S8, S9 and S10), indicating that the populations sorted by FCM from our incubations were not distorted. The one exception was picoeukaryotes, where filtered samples showed an increase in Chloropicophyceae (primarily *Chloroparvula pacifica*) relative abundance in cycles SA1 and SA2 to a median proportion of reads of 12% (Table S9), while its median proportion in sorted samples from SA1 and SA2 was 1.3%.

# Discussion

## High contribution of small phytoplankton toward productivity in the STFZ

Small phytoplankton (pico and nano size fractions) were important contributors to photosynthetic biomass in the STFZ zone during the spring time of this study, comprising at least 85% of total Chl *a* biomass (Figure S6) in all cycles except coastal SA-Sc (Décima et al. 2023). These results are consistent with previous measurements in the same area (Bradford-Grieve et al. 1997; Hall et al. 1999; McKay et al. 2005). The phytoplankton community in SA cycles were likely iron limited, especially in SA1 and SA2 with lower photochemical efficiency of photosystem II (Fv/Fm) and higher reoxidation kinetics ($Q_a^-$ lifetime) compared to ST cycles (see Décima et al. 2023, Figure 2C, corresponding to 'Salp SA' and 'Non-salp SA' cycles) consistent with physiological evidence reported in SA waters of this region (Boyd et al. 1999). Under nutrient limited conditions, smaller phytoplankton have an advantage over larger phytoplankton, as they have greater nutrient affinity and lower transport limitation for macronutrients (Pasciak and Gavis 1974; Raven 1998) and micronutrients (Franck et al. 2003; Hudson and Morel 1990; Marchetti and Cassar 2009). Additionally, in HNLC conditions, smaller cells are hypothesized to be less sensitive to iron-limited conditions as they have lower cell quotas for iron (Barber and Hiscock 2006; Morel et al. 1991).

SA-Sc had the highest relative contribution of microphytoplankton toward Chl *a* biomass (45%), accompanied by the second highest integrated NPP (Figure 2). The higher contribution microphytoplankton like diatoms (based on chemotaxonomic pigment analysis; Gutiérrez-Rodríguez, in preparation) in SA-Sc compared to oceanic SA cycles, as well as higher Fv/Fm and lower $Q_a^-$ lifetime values suggest an alleviation of HNLC conditions in SA-Sc stations possibly due to the influence of the Southland Current (Nodder et al. 2007), as described in Décima et al. (2023).

Our experiments showed that within small phytoplankton populations, nanoeukaryotes contributed most to productivity compared to *Synechococcus* and picoeukaryotes combined across all cycles except ST1, despite its lower cell abundance and contribution to Chl *a* biomass (Table 1). Jardillier et al. (2010) and Irion et al. (2021) suggest the carbon fixation by small phytoplankton (<20 µm) is dominated by cells with a diameter of 2-3 µm, smaller than nanoeukaryotes size in this study (average diameter of 3.61 µm), but nevertheless indicate intermediate sizes of phytoplankton have higher contribution toward NPP compared to picophytoplankton. Although *Synechococcus* had a higher cell abundance compared to picoeukaryotes, the contribution of picoeukaryotes and picocyanobacteria to productivity are comparable across a variety of open ocean conditions, including tropical and subtrop-

ical latitudes with oligotrophic and mesotrophic conditions (Jardillier et al. 2010; Li 1994; Rii et al. 2016b), and iron-limited SA waters of this study (Figure 3B and Table 1).

**Comparable variation of cell-specific carbon fixation rates with the literature**

Despite the variation in cell-specific carbon fixation rates between some replicates or experiments conducted within the same cycle (Figure S2), these rates were consistent with the range and the group-specific trends reported in previous studies (Figure 6 and Table S11). On one hand, the high variation in carbon fixation rates revealed by nanoSIMS single-cell measurements (Berthelot et al. 2019; Duerschlag et al. 2021; Irion et al. 2021) suggests that part of the variation we observed likely reflects true biological variability intrinsic to natural population dynamics and its adaptive capability to diverse environmental conditions (Olofsson et al. 2019). On the other hand, the systematically lower cell-specific carbon fixation rates exhibited by *Synechococcus* compared to photosynthetic pico- and nano-eukaryotes in both ST and SA cycles, has been reported in warmer tropical (Duhamel et al. 2019; Grob et al. 2011; Hartmann et al. 2014; Jardillier et al. 2010; Zubkov 2014) and colder Antarctic regions (Irion et al. 2021) (Figure 6) reinforcing the consistency of this size-dependent pattern.

*Synechococcus* and picoeukaryotes cell-specific carbon fixation rates were on the lower end of previously published rates (Figure 6). This was particularly marked for *Synechococcus* rates measured in SA waters. Previous studies mostly measured cell-specific carbon fixation rates across oligotrophic and mesotrophic conditions (Table S11), while this study was conducted mainly in oligotrophic conditions with low macronutrient concentrations (surface mixed layer $NO_3 \approx 1$ µM in ST ; Figure S5E), or high macronutrient concentrations ($NO_3 \approx 3$ µM in SA) but low iron concentrations, characteristic of iron-limited HNLC conditions, which could have capped cell-specific carbon fixation rates (Berthelot et al. 2019; Duerschlag et al. 2021; Rii et al. 2016b). Additionally, this study was conducted at a higher latitude with lower sea surface temperatures (excluding Irion et al. 2021), which might have resulted in lower cell-specific carbon fixation rates and growth rates (Barton et al. 2020; Chen et al. 2014; Fernández-González and Marañón 2021). For example, Hartmann et al. (2014) observed cell-specific carbon fixation rates of *Synechococcus* and picoeukaryotes decreased from the equatorial region to the southern temperate region. Therefore, we consider that the relatively low rates of *Synechococcus* and picoeukaryote populations measured in our study compared with previous ones a reflection of the oligotrophic conditions and lower temperatures found by these populations in the environment sampled.

In contrast, the cell-specific carbon fixation rates of nanoeukaryotes in our study were within the same

range of values as reported by the only other study measuring rates of nanoeukaryotes in the Southern Ocean (Irion et al. 2021) (Figure 6).

**Variation of cell-specific carbon fixation rates and the associated community across water masses**

The influence of taxonomic affiliation on cell-specific carbon fixation rates is often overlooked (Duhamel et al. 2019; Rii et al. 2016b). We assessed the taxonomic composition of the small phytoplankton populations of different domains (picocyanobacteria and eukaryotes) and sizes (pico and nano) in $^{14}$C-fixation experiments using a combination of FCM-sorting and DNA metabarcoding. Metabarcoding sequencing of sorted populations has revealed distinct community composition between ST and SA waters for each phytoplankton group, as well as between eukaryotic pico and nano phytoplankton populations (Figure 4). There were no significant differences in cell size (based on cell diameter and assuming a spherical shape) across all three groups between ST and SA cycles, nor was light likely a limiting factor (PAR profiles between the cycles were similar; Figure S5C). Therefore, the comparison of cell-specific carbon fixation rates between warm, macronutrient-limited ST cycles, and colder, iron-limited SA cycles were likely a reflection of intrinsic carbon-based growth rates affected by temperature (Boyd et al. 2013; Chen et al. 2014; Fernández-González and Marañón 2021) and nutrient availability (Gall et al. 2001; Irion et al. 2021), as well as taxa-specific responses (Buitenhuis et al. 2008; Caputi et al. 2019; Villiot et al. 2023).

The cell-specific carbon fixation rates and growth rates of photosynthetic pico- and nano-eukaryotes did not significantly differ between the water masses (Figure 3A,C), suggesting changes in sea surface temperature and iron concentration had no significant influence on the cell-specific carbon fixation rates and growth rates of small photosynthetic eukaryotes in this study. We did not expect temperature change in this study to affect the rates of small eukaryotes. The change in SST (3°C) from ST to SA cycles was smaller than the range considered in the studies where temperature was recorded to affect eukaryotic phytoplankton growth and metabolic rate (Fernández-González et al. 2022; López-Sandoval et al. 2021; Marañón et al. 2014, 2018), if they were even observed (Landry et al. 2022). Moreover, most of the taxa present in both ST and SA cycles are abundant or have high growth rates in temperatures that are similar or colder than that of SA conditions (Gutiérrez-Rodríguez et al. 2022; Irion et al. 2020; Leconte et al. 2020; Limardo et al. 2017; Medlin et al. 1994; Sow et al. 2020; Zhu et al. 2016). While there have been no studies comparing the cell-specific carbon fixation rates of small phytoplankton across macronutrient limited and iron limited conditions, a comparison

between iron limited and nutrient replete conditions in the Southern Ocean suggested lower growth rates for picoeukaryotes but not nanoeukaryotes (see Irion et al. 2021, based on interquartile range of cell-specific growth rates).

The FCM-sorted picoeukaryote community in SA cycles (Prymnesiophyceae and Chrysophyceae) and nanoeukaryote community in both ST and SA cycles (Dinophyceae and Prymnesiophyceae) were dominated by taxa with reported phago-mixotrophic strategies (taxa that express, or have potential to express, phototrophy and phagotrophy, sensu Flynn et al. 2019), based on our analysis with Schneider et al. (2020) database (trophic assignment of each ASV can be found in Github) and recent gene-based model predictions for Prymneseiophyceae (Koppelle et al. 2022) (Figure 5A-C). In ST and coastal SA-Sc cycles, the picoeukaryotic community was dominated by Mamiellophyceae (*Bathycoccus*, *Micromonas* and *Ostreococcus*) while in oceanic SA cycles, the community was co-represented by reads belonging to mixotrophic taxa of Prymnesiophyceae and Chrysophyceae in addition to the phototrophic taxa Mamiellophyceae and Pelagophyceae (Figure 5A,B). These mixotrophic taxa are abundant in HNLC SO region, and known to be adapted to low iron conditions (Gutiérrez-Rodríguez et al. 2023; Irion et al. 2020; Thiele et al. 2014).

The picoeukaryote Chloropicophyceae (primarily *Chloroparvula pacifica*) was abundant in the filtered samples of SA cycles in this study and in HNLC SA waters of the same region (Gutiérrez-Rodríguez et al. 2022), but present in low relative abundance in sorted samples (Table S9). The underestimation of Chloropicophyceae in the sorted community is likely due to unsuccessful preservation of its cells, as the prevalence of Chloropicophyceae in meso- and oligotrophic open ocean waters in tropical to subtropical latitudes was originally described from live sorted populations (Moon-van der Staay et al. 2001; Shi et al. 2009), suggesting that physical sorting is not an issue for this group. Nevertheless, gene-based model predictions have suggested that the phago-mixotrophic is a trophic strategy present in two chloropicophycean strains analyzed in contrast with mamiellophyceans which were predicted as non-phagotrophs (Bock et al. 2021).

Dinophyceae and Prymnesiophyceae were dominant components of FCM-sorted nanoeukaryote populations across the range of environmental conditions surveyed (Figure 5C). Although Dinophyceae has a high copy number of ribosomal RNA (Zhu et al. 2005) that could lead to overestimation of its abundance within nanoeukaryotes, the presence of Dinophyceae across the cycles was also indicated by the proportion Peridinin to total Chl *a* biomass (2–6%) in Décima et al. (2023). Taxa within the major orders (Peridiniales, Gymnodiniales and Prorocentrales) and genera (*Karlodinium*, *Gyrodinium* and *Prorocentrum*) of Dinophyceae identified in our sorted dataset have been recorded as mixotrophic

(Burkholder et al. 2008; Li et al. 1999; Mitra et al. 2023; Schneider et al. 2020; Stoecker 1999; Stoecker et al. 2017). Unfortunately, a good proportion of reads (15.1%) and ASVs (11%) were assigned to Dinophyceae without a formal description, which impairs their assignment to trophic groups in the same way done for the others ASVs. It also suggests that there is still an important component of this photosynthetic nanoeukaryotic community yet to be described and characterized.

Within Prymnesiophyceae, *Gephyrocapsa huxleyi* and few taxa within *Chrysochromulina* sp. that were dominant in ST cycles (Figure S7) are also capable of phagotrophy (Avrahami and Frada 2020; Frias-Lopez et al. 2009; Li et al. 2022; Safi and Hall 1999). The presence of *Gephyrocapsa huxleyi* in the nano size fraction and prominence within cocolithophores in the region was previously confirmed by metabarcoding, microscopy and imaging studies (Chang and Northcote 2016; Gutiérrez-Rodríguez et al. 2022; Rigual-Hernández et al. 2020). Recent gene-based model predictions have suggested that the phago-mixotrophic is a trophic strategy present in several members of the *Phaeocystis*, *Chrysochromulina* and *Gephyrocapsa* genera and other haptophytes (Koppelle et al. 2022). *Phaeocystis antarctica* was the only taxa present in both picoeukaryote and nanoeukaryote populations represented by the same ASV (Figures 5B and S7). Size reduction has been indicated as one of the variable responses to iron limitation within clonal *Phaeocystis antarctica* culture populations, which could explain the presence of these taxa in both sorted populations (Luxem et al. 2017).

Other adaptations to low iron conditions besides phago-mixotrophy were likely present in the community, especially within phototrophic picoeukaryotes. Based on genome analysis, Pelagophyceae and *Phaeocystis antarctica* suggests a physiological advantage in iron uptake and storage (Guérin et al. 2022; Strzepek et al. 2011). Mamiellophyceae species *Bathycoccus prasinos* is suggested to overcome iron limitation by nickel acquisition (Simmons et al. 2016).

The similar cell-specific carbon fixation rates observed for small photosynthetic eukaryotes between the water masses might be sustained by phago-mixotrophy strategy being deployed among the taxa described in our samples. While mixotrophy via osmotrophy is likely a ubiquitous trait amongst phytoplankton (as discussed by Mitra et al. 2023), the phago-mixotrophic strategy is a specific characteristic that can vary even within genus level taxonomic groups (Schneider et al. 2020). Phago-mixotrophy can increase the competitiveness of mixoplankton under macro and micro nutrient limited conditions by alleviating nutrient stress (Barton et al. 2013; Cohen et al. 2021; Edwards 2019; Stukel et al. 2011), even with increased metabolic cost of maintaining biomass for both autotrophy and phagotrophy (Ward et al. 2011). Small mixoplankton flagellates (3–5 µm) carry out at least 40% of bactivory in both oligotrophic and HNLC conditions (Stukel et al. 2011; Zubkov and Tarran 2008). Grazing is

also important to regenerate iron in HNLC conditions (Strzepek et al. 2005), possibly making iron more bioavailable in the water mass. Duhamel et al. (2019) reported that small eukaryotes (< 5 µm), where Dinophyceae were present, had low uptake of phosphate in oligotrophic conditions despite high biomass-normalised carbon fixation rates. The authors suggested phago-mixotrophy as a way for small eukaryotes to overcome macronutrient limitation, and we show that this strategy was present in distinct pico and nanoeukaryote populations in micronutrient-limited conditions, whereas in macronutrient-limited conditions, only the nanoeukaryote population was dominated by phago-mixotrophic taxa. Interestingly, although both small eukaryotic communities were dominated by phago-mixoplankton in SA cycles, nanoeukaryotes had higher growth rates than picoeukyarotes, suggesting nanoeukaryotes were more competitive than picoeukaryotes (Figure 3C). Whereas in ST cycles, picoeukaryotes with a dominant phototrophic community and nanoeukaryotes with a phago-mixotrophic community had similar growth rates, suggesting equally competitive populations.

In contrast to small eukaryotes, *Synechococcus* had a 3-fold decrease in cell-specific carbon fixation rate and growth rate from ST to SA cycles (Figure 3A,C). *Synechococcus* was equally competitive against small eukaryotes in ST cycles with no difference in growth rates, while in SA cycles had the lowest growth rates (Figure 3C). The lower cell-specific carbon fixation rates and growth rates in SA cycles could be partly due to cold-adapted ecotypes having lower maximal growth rates under the temperature conditions found during SA cycles. The growth rate of *Synechococcus* is tightly coupled to temperature (Landry et al. 2022), especially from winter to spring (Hunter-Cevera et al. 2020, 2014). DNA metabarcoding analysis revealed *Synechococcus* sorted populations were dominated by clades I and IV (Figure 5D), which have been shown to be associated with cold, open ocean and coastal waters at latitudes above 30°N and below 30°S (Huang et al. 2012; Kent et al. 2019; Mazard et al. 2012; Sohm et al. 2016; Xia et al. 2019; Zwirglmaier et al. 2008) and dominate the community at temperatures similar to this study (10–15°C) (Farrant et al. 2016). However, strains of clade I isolated at 12–13°C are suggested as not true psychrophilic phytoplankton, as their optimal temperature for growth (about 22 °C) was higher than their original environment (Pittera et al. 2014).

Changes in the community composition of *Synechococcus* from ST to SA cycles suggested a shift towards ecotypes described in, and therefore possibly adapted, to low iron conditions. Yet, the low cell-specific carbon fixation rates and growth rates of this group observed in HNLC waters might indicate that *Synechococcus* populations in SA cycles were likely also limited by iron availability in addition to low temperatures, as described above. The environmental niche of *Synechococcus* at subclade level is not yet well-defined, but the distribution of subclades seems to exhibit environmental preferences (Farrant et al. 2016; Hunter-Cevera et al. 2016). Subclades IVa and IVb were dominant in

ST and SA cycles, respectively (Figure 5D). Farrant et al. (2016) suggests subclade IVa (corresponding to Ecologically Significant Taxonomic Unit (ESTU) IVA) thrives in cold conditions where iron is not limiting. While there is no agreement on the niche of subclade IVb (corresponding to ESTU IVC in Farrant et al. 2016), our results indicate that it is at least tolerant of iron-limited conditions. Whole genome analysis found siderophore uptake genes in clade IV (Hogle et al. 2022), suggesting clade IV can adapt to low iron conditions by directly taking up siderophores (iron molecules bound to ligands) instead of dissolved iron. Despite these adaptations, *Synechococcus* communities dominating in iron limited conditions can still exhibit signs of iron stress (Gilbert et al. 2022) and be co-limited by other elements such as trace metals (Goes et al. 2016).

Although *Synechococcus* had 3-fold lower cell-specific carbon fixation rates in SA compared to ST waters, the group-specific productivity of *Synechococcus* was not significantly different between the water masses (based on model estimations, Table S5) as *Synechococcus* had higher cell abundance in SA waters. The greater accumulation of *Synechococcus* in SA compared to ST waters, despite lower growth rates, could be the result of a decoupling between growth and loss rates from grazing and viral lysis. Hunter-Cevera et al. (2020) recorded a small uncoupling between growth and loss rates at the start of the spring bloom, allowing for accumulation of *Synechococcus* at the Martha's Vineyard Coastal Observatory (North Atlantic). As lower temperature is associated with lower grazing (Rose and Caron 2007) and viral lysis rates (Mojica et al. 2016), *Synechococcus* could have lower loss rates in SA waters compared to ST waters, leading to a greater accumulation. Alternatively, *Synechococcus* might have high standing stock in the region, as it also had similar abundance at the nearby Bounty Trough region (47°S and 170°E) during autumn (Gutiérrez-Rodríguez et al. 2020), when decoupling between growth and loss rates which occurred during spring and summer periods are expected to rebalance (Hunter-Cevera et al. 2020). Future studies that jointly assess the taxonomic composition of marine *Synechococcus* at fine-scales and their cellular physiology by direct *in situ* measurements are needed to further improve our understanding of the ecological traits associated with the successful distribution of this group across contrasting oceanic regions. To our knowledge, this is the first study providing *in situ* carbon fixation rates of *Synechococcus* populations taxonomically characterized at subclade level.

We did not observe depth partitioning between the surface and DCM for all three phytoplankton populations for carbon fixation rates (fgC cell$^{-1}$ h $^{-1}$), group-specific productivity (mgC m$^{-3}$ day$^{-1}$), growth rates (day $^{-1}$) and taxonomic composition (Table S6). This could be partly due to the lower number of samples collected from the DCM (4–5 out of 11 incubation experiments; Table S6) because of sampling limitations. Previous studies have revealed niche partitioning in carbon fixation rates and

community composition between picocyanobacteria and picoeukaryotes (Duerschlag et al. 2021; Rii et al. 2016b), which we cannot rule out in our study.

# Conclusion

In conclusion, small phytoplankton contributed to a large proportion of phytoplankton biomass and total primary production across oligotrophic ST to HNLC SA waters in the southwest Pacific Ocean. Although *Synechococcus* had lower cell-specific carbon fixation rates in HNLC SA compared to ST waters, the group-specific productivity remained the same due to high cell abundance. Pico and nanoeukaryote populations had no significant difference in cell-specific carbon fixation rates despite changes from macro to micro-nutrient limited conditions. A closer look at the taxonomic composition suggests phago-mixotrophy as a strategy to adapt to iron limited conditions amongst distinct pico and nanoeukaryote populations. As cell-specific carbon fixation rates of small phytoplankton are still poorly constrained, we need further measurements paired with taxonomic identification to understand the variation of small photosynthetic eukaryotes across more environmental conditions.

# References cited

Amante, C. and B. W. Eakins (2009). *ETOPO1 1 Arc-Minute Global Relief Model Procedures, Data Sources and Analysis*. NOAA Technical Memorandum NESDIS NGDC-24. National Geophysical Data Center, NOAA, 25.

Anderson, M. J. and D. C. I. Walsh (2013). PERMANOVA, ANOSIM, and the Mantel Test in the Face of Heterogeneous Dispersions: What Null Hypothesis Are You Testing? *Ecological Monographs* 83, 557–574.

Avrahami, Y. and M. J. Frada (2020). Detection of Phagotrophy in the Marine Phytoplankton Group of the Coccolithophores (Calcihaptophycidae, Haptophyta) During Nutrient-replete and Phosphate-limited Growth. *Journal of Phycology* 56, 1103–1108.

Barber, R. T. and M. R. Hiscock (2006). A Rising Tide Lifts All Phytoplankton: Growth Response of Other Phytoplankton Taxa in Diatom-Dominated Blooms. *Global Biogeochemical Cycles* 20.

Barton, A. D., Z. V. Finkel, B. A. Ward, D. G. Johns, and M. J. Follows (2013). On the Roles of Cell Size and Trophic Strategy in North Atlantic Diatom and Dinoflagellate Communities. *Limnology and Oceanography* 58, 254–266.

Barton, S., J. Jenkins, A. Buckling, C.-E. Schaum, N. Smirnoff, J. A. Raven, and G. Yvon-Durocher (2020). Evolutionary Temperature Compensation of Carbon Fixation in Marine Phytoplankton. *Ecology Letters* 23, 722–733.

Bendif, E. M., B. Nevado, E. L. Y. Wong, K. Hagino, I. Probert, J. R. Young, R. E. M. Rickaby, and D. A. Filatov (2019). Repeated Species Radiations in the Recent Evolution of the Key Marine Phytoplankton Lineage Gephyrocapsa. *Nature Communications* 10, 4234.

Berthelot, H., S. Duhamel, S. L'Helguen, J.-F. Maguer, S. Wang, I. Cetini, and N. Cassar (2019). NanoSIMS Single Cell Analyses Reveal the Contrasting Nitrogen Sources for Small Phytoplankton. *The ISME Journal* 13, 651–662.

Berthelot, H., S. Duhamel, S. L'Helguen, J.-F. Maguer, and N. Cassar (2021). Inorganic and Organic Carbon and Nitrogen Uptake Strategies of Picoplankton Groups in the Northwestern Atlantic Ocean. *Limnology and Oceanography* 66, 3682–3696.

Bertilsson, S., O. Berglund, D. M. Karl, and S. W. Chisholm (2003). Elemental Composition of Marine *Prochlorococcus* and *Synechococcus* : Implications for the Ecological Stoichiometry of the Sea. *Limnology and Oceanography* 48, 1721–1731.

Bock, N. A., S. Charvet, J. Burns, Y. Gyaltshen, A. Rozenberg, S. Duhamel, and E. Kim (2021). Experimental Identification and in Silico Prediction of Bacterivory in Green Algae. *The ISME Journal* 15, 1987–2000.

Boyd, P., J. LaRoche, M. Gall, R. Frew, and R. M. L. McKay (1999). Role of Iron, Light, and Silicate in Controlling Algal Biomass in Subantarctic Waters SE of New Zealand. *Journal of Geophysical Research: Oceans* 104, 13395–13408.

Boyd, P. W., T. A. Rynearson, E. A. Armstrong, F. Fu, K. Hayashi, Z. Hu, D. A. Hutchins, R. M. Kudela, E. Litchman, M. R. Mulholland, U. Passow, R. F. Strzepek, K. A. Whittaker, E. Yu, and M. K. Thomas (2013). Marine Phytoplankton Temperature versus Growth Responses from Polar to Tropical Waters  Outcome of a Scientific Community-Wide Study. *PLOS ONE* 8, e63091.

Boyd, P. W., R. Strzepek, F. Fu, and D. A. Hutchins (2010). Environmental Control of Open-Ocean Phytoplankton Groups: Now and in the Future. *Limnology and Oceanography* 55, 1353–1376.

Boyd, P. W. et al. (2000). A Mesoscale Phytoplankton Bloom in the Polar Southern Ocean Stimulated by Iron Fertilization. *Nature* 407, 695–702.

Bradford-Grieve, J. M., F. H. Chang, M. Gall, S. Pickmere, and F. Richards (1997). Size-fractionated Phytoplankton Standing Stocks and Primary Production during Austral Winter and Spring 1993 in the Subtropical Convergence Region near New Zealand. *New Zealand Journal of Marine and Freshwater Research* 31, 201–224.

Buitenhuis, E. T., T. Pangerc, D. J. Franklin, C. Le Quéré, and G. Malin (2008). Growth Rates of Six Coccolithophorid Strains as a Function of Temperature. *Limnology and Oceanography* 53, 1181–1185.

Burkholder, J. M., P. M. Glibert, and H. M. Skelton (2008). Mixotrophy, a major mode of nutrition for harmful algal species in eutrophic waters. *Harmful Algae* 8. HABs and Eutrophication, 77–93.

Callahan, B. J., P. J. McMurdie, M. J. Rosen, A. W. Han, A. J. A. Johnson, and S. P. Holmes (2016). DADA2: High-resolution Sample Inference from Illumina Amplicon Data. *Nature Methods* 13, 581–583.

Caputi, L. et al. (2019). Community-Level Responses to Iron Availability in Open Ocean Plankton Ecosystems. *Global Biogeochemical Cycles* 33, 391–419.

Cavender-Bares, J., K. H. Kozak, P. V. A. Fine, and S. W. Kembel (2009). The Merging of Community Ecology and Phylogenetic Biology. *Ecology Letters* 12, 693–715.

Chang, F. H. and L. Northcote (2016). Species Composition of Extant Coccolithophores Including Twenty Six New Records from the Southwest Pacific near New Zealand. *Marine Biodiversity Records* 9, 75.

Chen, B., H. Liu, B. Huang, and J. Wang (2014). Temperature Effects on the Growth Rate of Marine Picoplankton. *Marine Ecology Progress Series* 505, 37–47.

Chiswell, S. M., H. C. Bostock, P. J. Sutton, and M. J. Williams (2015). Physical Oceanography of the Deep Seas around New Zealand: A Review. *New Zealand Journal of Marine and Freshwater Research* 49, 286–317.

Chiswell, S. M., A. Gutiérrez-Rodríguez, M. Gall, K. Safi, R. Strzepek, M. R. Décima, and S. D. Nodder (2022). Seasonal Cycles of Phytoplankton and Net Primary Production from Biogeochemical Argo Float Data in the South-West Pacific Ocean. *Deep Sea Research Part I: Oceanographic Research Papers* 187, 103834.

Cohen, N. R., M. R. McIlvin, D. M. Moran, N. A. Held, J. K. Saunders, N. J. Hawco, M. Brosnahan, G. R. DiTullio, C. Lamborg, J. P. McCrow, C. L. Dupont, A. E. Allen, and M. A. Saito (2021). Dinoflagellates Alter Their Carbon and Nutrient Metabolic Strategies across Environmental Gradients in the Central Pacific Ocean. *Nature Microbiology* 6, 173–186.

de Baar, H. J. W., J. T. M. de Jong, D. C. E. Bakker, B. M. Löscher, C. Veth, U. Bathmann, and V. Smetacek (1995). Importance of Iron for Plankton Blooms and Carbon Dioxide Drawdown in the Southern Ocean. *Nature* 373, 412–415.

De La Rocha, C. L. and U. Passow (2014). 8.4 - The Biological Pump. *Treatise on Geochemistry (Second Edition)*. Oxford, 93–122.

Décima, M., M. R. Stukel, S. D. Nodder, A. Gutiérrez-Rodríguez, K. E. Selph, A. L. dos Santos, K. Safi, T. B. Kelly, F. Deans, S. E. Morales, F. Baltar, M. Latasa, M. Y. Gorbunov, and M. Pinkerton (2023). Salp Blooms Drive Strong Increases in Passive Carbon Export in the Southern Ocean. *Nature Communications* 14, 425.

Duerschlag, J., W. Mohr, T. G. Ferdelman, J. LaRoche, D. Desai, P. L. Croot, D. VoSS, O. Zielinski, G. Lavik, S. Littmann, C. Martínez-Pérez, B. Tschitschko, N. Bartlau, H. Osterholz, T. Dittmar, and M. M. M. Kuypers (2021). Niche Partitioning by Photosynthetic Plankton as a Driver of CO2-fixation across the Oligotrophic South Pacific Subtropical Ocean. *The ISME Journal*, 1–12.

Dugdale, R. C., F. P. Wilkerson, and H. J. Minas (1995). The Role of a Silicate Pump in Driving New Production. *Deep Sea Research Part I: Oceanographic Research Papers* 42, 697–719.

Duhamel, S. and T. Moutin (2009). Carbon and Phosphate Incorporation Rates of Microbial Assemblages in Contrasting Environments in the Southeast Pacific. *Marine Ecology Progress Series* 375, 53–64.

Duhamel, S., E. Kim, B. Sprung, and O. R. Anderson (2019). Small Pigmented Eukaryotes Play a Major Role in Carbon Cycling in the P-depleted Western Subtropical North Atlantic, Which May Be Supported by Mixotrophy. *Limnology and Oceanography* 64, 2424–2440.

Edwards, K. F. (2019). Mixotrophy in Nanoflagellates across Environmental Gradients in the Ocean. *Proceedings of the National Academy of Sciences of the United States of America* 116, 6211–6220.

Falkowski, P. G., R. T. Barber, and V. Smetacek (1998). Biogeochemical Controls and Feedbacks on Ocean Primary Production. *Science* 281, 200–206.

Farrant, G. K., H. Doré, F. M. Cornejo-Castillo, F. Partensky, M. Ratin, M. Ostrowski, F. D. Pitt, P. Wincker, D. J. Scanlan, D. Iudicone, S. G. Acinas, and L. Garczarek (2016). Delineating Ecologically Significant Taxonomic Units from Global Patterns of Marine Picocyanobacteria. *Proceedings of the National Academy of Sciences* 113, E3365–E3374.

Fernández-González, C. and E. Marañón (2021). Effect of Temperature on the Unimodal Size Scaling of Phytoplankton Growth. *Scientific Reports* 11, 953.

Fernández-González, C., G. A. Tarran, N. Schuback, E. M. S. Woodward, J. Arístegui, and E. Marañón (2022). Phytoplankton Responses to Changing Temperature and Nutrient Availability Are Consistent across the Tropical and Subtropical Atlantic. *Communications Biology* 5, 1–13.

Field, C. B., M. J. Behrenfeld, J. T. Randerson, and P. Falkowski (1998). Primary Production of the Biosphere: Integrating Terrestrial and Oceanic Components. *Science* 281, 237–240.

Flynn, K. J. et al. (2019). Mixotrophic protists and a new paradigm for marine ecology: where does plankton research go now? *Journal of Plankton Research* 41, 375–391.

Flynn, R. F., L. Haraguchi, J. McQuaid, J. M. Burger, P. Mutseka Lunga, L. Stirnimann, S. Samanta, A. N. Roychoudhury, and S. E. Fawcett (2023). Nanoplankton: The Dominant Vector for Carbon Export across the Atlantic Southern Ocean in Spring. *Science Advances* 9, eadi3059.

Fox, J. and S. Weisberg (2019). *An R Companion to Applied Regression*. Third. Thousand Oaks CA.

Franck, V. M., K. W. Bruland, D. A. Hutchins, and M. A. Brzezinski (2003). Iron and Zinc Effects on Silicic Acid and Nitrate Uptake Kinetics in Three High-Nutrient, Low-Chlorophyll (HNLC) Regions. *Marine Ecology Progress Series* 252, 15–33.

Frias-Lopez, J., A. Thompson, J. Waldbauer, and S. W. Chisholm (2009). Use of Stable Isotope-Labelled Cells to Identify Active Grazers of Picocyanobacteria in Ocean Surface Waters. *Environmental Microbiology* 11, 512–525.

Frölicher, T. L., J. L. Sarmiento, D. J. Paynter, J. P. Dunne, J. P. Krasting, and M. Winton (2015). Dominance of the Southern Ocean in Anthropogenic Carbon and Heat Uptake in CMIP5 Models. *Journal of Climate* 28, 862–886.

Gall, M. P., R. Strzepek, M. Maldonado, and P. W. Boyd (2001). Phytoplankton Processes. Part 2: Rates of Primary Production and Factors Controlling Algal Growth during the Southern Ocean Iron RElease Experiment (SOIREE). *Deep Sea Research Part II: Topical Studies in Oceanography.* The Southern Ocean Iron Release Experiment (SOIREE) 48, 2571–2590.

Garcia, N., P. Raimbault, and V. Sandroni (2007). Seasonal Nitrogen Fixation and Primary Production in the Southwest Pacific: Nanoplankton Diazotrophy and Transfer of Nitrogen to Picoplankton Organisms. *Marine Ecology Progress Series* 343, 25–33.

Gérikas Ribeiro, C., A. Lopes dos Santos, D. Marie, F. Pereira Brandini, and D. Vaulot (2018). Small Eukaryotic Phytoplankton Communities in Tropical Waters off Brazil Are Dominated by Symbioses between Haptophyta and Nitrogen-Fixing Cyanobacteria. *The ISME Journal* 12, 1360–1374.

Gilbert, N. E., G. R. LeCleir, R. F. Strzepek, M. J. Ellwood, B. S. Twining, S. Roux, C. Pennacchio, P. W. Boyd, and S. W. Wilhelm (2022). Bioavailable Iron Titrations Reveal Oceanic *Synechococcus* Ecotypes Optimized for Different Iron Availabilities. *ISME Communications* 2, 1–12.

Goes, J. I., H. d. R. Gomes, K. E. Selph, and M. R. Landry (2016). Biological Response of Costa Rica Dome Phytoplankton to Light, Silicic Acid and Trace Metals. *Journal of Plankton Research* 38, 290–304.

Grob, C., M. Hartmann, M. V. Zubkov, and D. J. Scanlan (2011). Invariable Biomass-Specific Primary Production of Taxonomically Discrete Picoeukaryote Groups across the Atlantic Ocean. *Environmental Microbiology* 13, 3266–3274.

Grob, C., L. Jardillier, M. Hartmann, M. Ostrowski, M. V. Zubkov, and D. J. Scanlan (2015). Cell-Specific $CO_2$ Fixation Rates of Two Distinct Groups of Plastidic Protists in the Atlantic Ocean Remain Unchanged after Nutrient Addition. *Environmental Microbiology Reports* 7, 211–218.

Guérin, N., M. Ciccarella, E. Flamant, P. Frémont, S. Mangenot, B. Istace, B. Noel, C. Belser, L. Bertrand, K. Labadie, C. Cruaud, S. Romac, C. Bachy, M. Gachenot, E. Pelletier, A. Alberti, O. Jaillon, P. Wincker, J.-M. Aury, and Q. Carradec (2022). Genomic Adaptation of the Picoeukaryote Pelagomonas Calceolata to Iron-Poor Oceans Revealed by a Chromosome-Scale Genome Sequence. *Communications Biology* 5, 1–14.

Guillou, L. et al. (2013). The Protist Ribosomal Reference Database (PR2): A Catalog of Unicellular Eukaryote Small Sub-Unit rRNA Sequences with Curated Taxonomy. *Nucleic Acids Research* 41, D597–D604.

Gutiérrez-Rodríguez, A., K. Safi, D. Fernández, A. Forcén-Vázquez, P. Gourvil, L. Hoffmann, M. Pinkerton, P. Sutton, and S. D. Nodder (2020). Decoupling Between Phytoplankton Growth and

Microzooplankton Grazing Enhances Productivity in Subantarctic Waters on Campbell Plateau, Southeast of New Zealand. *Journal of Geophysical Research: Oceans* 125, e2019JC015550.

Gutiérrez-Rodríguez, A., M. Latasa, K. Safi, M. H. Pinkerton, and S. D. Nodder (2023). Decoupled Growth and Grazing Rates of Diatoms and Green Algae Drive Increased Phytoplankton Productivity on HNLC Sub-Antarctic Plateaux. *Limnology and Oceanography Letters* n/a ().

Gutiérrez-Rodríguez, A., A. Lopes dos Santos, K. Safi, I. Probert, F. Not, D. Fernández, P. Gourvil, J. Bilewitch, D. Hulston, M. Pinkerton, and S. D. Nodder (2022). Planktonic Protist Diversity across Contrasting Subtropical and Subantarctic Waters of the Southwest Pacific. *Progress in Oceanography* 206, 102809.

Hall, J. A., M. R. James, and J. M. Bradford-Grieve (1999). Structure and Dynamics of the Pelagic Microbial Food Web of the Subtropical Convergence Region East of New Zealand. *Aquatic Microbial Ecology* 20, 95–105.

Hartmann, M., P. Gomez-Pereira, C. Grob, M. Ostrowski, D. J. Scanlan, and M. V. Zubkov (2014). Efficient $CO_2$ Fixation by Surface *Prochlorococcus* in the Atlantic Ocean. *The ISME Journal* 8, 2280–2289.

Hogle, S. L., T. Hackl, R. M. Bundy, J. Park, B. Satinsky, T. Hiltunen, S. Biller, P. M. Berube, and S. W. Chisholm (2022). Siderophores as an Iron Source for Picocyanobacteria in Deep Chlorophyll Maximum Layers of the Oligotrophic Ocean. *The ISME Journal* 16, 1636–1646.

Huang, S., S. W. Wilhelm, H. R. Harvey, K. Taylor, N. Jiao, and F. Chen (2012). Novel Lineages of *Prochlorococcus* and *Synechococcus* in the Global Oceans. *The ISME Journal* 6, 285–297.

Hudson, R. J. M. and F. M. M. Morel (1990). Lron Transport in Marine Phytoplankton: Kinetics of Cellular and Medium Coordination Reactions. *Limnology and Oceanography* 35, 1002–1020.

Hunter-Cevera, K. R., M. G. Neubert, R. J. Olson, A. Shalapyonok, A. R. Solow, and H. M. Sosik (2020). Seasons of Syn. *Limnology and Oceanography* 65, 1085–1102.

Hunter-Cevera, K. R., M. G. Neubert, A. R. Solow, R. J. Olson, A. Shalapyonok, and H. M. Sosik (2014). Diel Size Distributions Reveal Seasonal Growth Dynamics of a Coastal Phytoplankter. *Proceedings of the National Academy of Sciences* 111, 9852–9857.

Hunter-Cevera, K. R., A. F. Post, E. E. Peacock, and H. M. Sosik (2016). Diversity of *Synechococcus* at the Martha's Vineyard Coastal Observatory: Insights from Culture Isolations, Clone Libraries, and Flow Cytometry. *Microbial Ecology* 71, 276–289.

Irion, S., U. Christaki, H. Berthelot, S. L'Helguen, and L. Jardillier (2021). Small Phytoplankton Contribute Greatly to $CO_2$-fixation after the Diatom Bloom in the Southern Ocean. *The ISME Journal*.

Irion, S., L. Jardillier, I. Sassenhagen, and U. Christaki (2020). Marked Spatiotemporal Variations in Small Phytoplankton Structure in Contrasted Waters of the Southern Ocean (Kerguelen Area). *Limnology and Oceanography* 65, 2835–2852.

Jardillier, L., M. V. Zubkov, J. Pearman, and D. J. Scanlan (2010). Significant CO2 Fixation by Small Prymnesiophytes in the Subtropical and Tropical Northeast Atlantic Ocean. *The ISME Journal* 4, 1180–1192.

Kent, A. G., S. E. Baer, C. Mouginot, J. S. Huang, A. A. Larkin, M. W. Lomas, and A. C. Martiny (2019). Parallel Phylogeography of *Prochlorococcus* and *Synechococcus*. *The ISME Journal* 13, 430–441.

Koppelle, S., D. López-Escardó, C. P. Brussaard, J. Huisman, C. J. Philippart, R. Massana, and S. Wilken (2022). Mixotrophy in the bloom-forming genus Phaeocystis and other haptophytes. *Harmful Algae* 117, 102292.

Landry, M. R., M. D. Ohman, R. Goericke, M. R. Stukel, and K. Tsyrklevich (2009). Lagrangian Studies of Phytoplankton Growth and Grazing Relationships in a Coastal Upwelling Ecosystem off Southern California. *Progress in Oceanography* 83, 208–216.

Landry, M. R., K. E. Selph, R. R. Hood, C. H. Davies, and L. E. Beckley (2022). Low Temperature Sensitivity of Picophytoplankton P : B Ratios and Growth Rates across a Natural 10řC Temperature Gradient in the Oligotrophic Indian Ocean. *Limnology and Oceanography Letters* 7, 112–121.

Larsson, U. and Å. Hagström (1982). Fractionated Phytoplankton Primary Production, Exudate Release and Bacterial Production in a Baltic Eutrophication Gradient. *Marine Biology* 67, 57–70.

Leconte, J., L. F. Benites, T. Vannier, P. Wincker, G. Piganeau, and O. Jaillon (2020). Genome Resolved Biogeography of Mamiellales. *Genes* 11, 66.

Lenth, R. V. (2023). *emmeans: Estimated Marginal Means, aka Least-Squares Means*. R package version 1.8.7.

Lepere, C., M. Demura, M. Kawachi, S. Romac, I. Probert, and D. Vaulot (2011). Whole-Genome Amplification (WGA) of Marine Photosynthetic Eukaryote Populations. *FEMS Microbiology Ecology* 76, 513–523.

Li, A., D. K. Stoecker, and J. E. Adolf (1999). Feeding, Pigmentation, Photosynthesis and Growth of the Mixotrophic Dinoflagellate *Gyrodinium Galatheanum*. *Aquatic Microbial Ecology* 19, 163–176.

Li, Q., K. F. Edwards, C. R. Schvarcz, and G. F. Steward (2022). Broad Phylogenetic and Functional Diversity among Mixotrophic Consumers of *Prochlorococcus*. *The ISME Journal* 16, 1557–1569.

Li, W. K. W. (1994). Primary Production of Prochlorophytes, Cyanobacteria, and Eucaryotic Ultraphytoplankton: Measurements from Flow Cytometric Sorting. *Limnology and Oceanography* 39, 169–175.

Limardo, A. J., S. Sudek, C. J. Choi, C. Poirier, Y. M. Rii, M. Blum, R. Roth, U. Goodenough, M. J. Church, and A. Z. Worden (2017). Quantitative Biogeography of Picoprasinophytes Establishes Ecotype Distributions and Significant Contributions to Marine Phytoplankton. *Environmental Microbiology* 19, 3219–3234.

Litchman, E., P. de Tezanos Pinto, C. A. Klausmeier, M. K. Thomas, and K. Yoshiyama (2010). Linking Traits to Species Diversity and Community Structure in Phytoplankton. *Hydrobiologia* 653, 15–28.

Logares, R., I. M. Deutschmann, P. C. Junger, C. R. Giner, A. K. Krabberød, T. S. B. Schmidt, L. Rubinat-Ripoll, M. Mestre, G. Salazar, C. Ruiz-González, M. Sebastián, C. de Vargas, S. G. Acinas, C. M. Duarte, J. M. Gasol, and R. Massana (2020). Disentangling the Mechanisms Shaping the Surface Ocean Microbiota. *Microbiome* 8, 55.

López-Sandoval, D. C., C. M. Duarte, and S. Agustí (2021). Nutrient and Temperature Constraints on Primary Production and Net Phytoplankton Growth in a Tropical Ecosystem. *Limnology and Oceanography* 66, 2923–2935.

Lüdecke, D. (2018). Ggeffects: Tidy Data Frames of Marginal Effects from Regression Models. *Journal of Open Source Software* 3, 772.

Luxem, K. E., M. J. Ellwood, and R. F. Strzepek (2017). Intraspecific Variability in Phaeocystis Antarctica's Response to Iron and Light Stress. *PLOS ONE* 12, e0179751.

Marañón, E., P. Cermeño, M. Huete-Ortega, D. C. López-Sandoval, B. Mouriño-Carballido, and T. Rodríguez-Ramos (2014). Resource Supply Overrides Temperature as a Controlling Factor of Marine Phytoplankton Growth. *PLOS ONE* 9, e99312.

Marañón, E., M. P. Lorenzo, P. Cermeño, and B. Mouriño-Carballido (2018). Nutrient Limitation Suppresses the Temperature Dependence of Phytoplankton Metabolic Rates. *The ISME Journal* 12, 1836–1845.

Marchetti, A. and N. Cassar (2009). Diatom Elemental and Morphological Changes in Response to Iron Limitation: A Brief Review with Potential Paleoceanographic Applications. *Geobiology* 7, 419–431.

Marie, D., X. L. Shi, F. Rigaut-Jalabert, and D. Vaulot (2010). Use of Flow Cytometric Sorting to Better Assess the Diversity of Small Photosynthetic Eukaryotes in the English Channel. *FEMS Microbiology Ecology* 72, 165–178.

Martin, M. (2011). Cutadapt Removes Adapter Sequences from High-Throughput Sequencing Reads. *EMBnet.journal* 17, 10–12.

Mazard, S., M. Ostrowski, F. Partensky, and D. J. Scanlan (2012). Multi-Locus Sequence Analysis, Taxonomic Resolution and Biogeography of Marine *Synechococcus*. *Environmental Microbiology* 14, 372–386.

McKay, R. M. L., S. W. Wilhelm, J. Hall, D. A. Hutchins, M. M. D. Al-Rshaidat, C. E. Mioni, S. Pickmere, D. Porta, and P. W. Boyd (2005). Impact of Phytoplankton on the Biogeochemical Cycling of Iron in Subantarctic Waters Southeast of New Zealand during FeCycle. *Global Biogeochemical Cycles* 19.

McMurdie, P. J. and S. Holmes (2013). Phyloseq: An R Package for Reproducible Interactive Analysis and Graphics of Microbiome Census Data. *PLOS ONE* 8, e61217.

Medlin, L. K., M. Lange, and M. E. M. Baumann (1994). Genetic Differentiation among Three Colony-Forming Species of Phaeocystis: Further Evidence for the Phylogeny of the Prymnesiophyta. *Phycologia* 33, 199–212.

Menden-Deuer, S. and E. J. Lessard (2000). Carbon to Volume Relationships for Dinoflagellates, Diatoms, and Other Protist Plankton. *Limnology and Oceanography* 45, 569–579.

Mitra, A., D. A. Caron, E. Faure, K. J. Flynn, S. G. Leles, P. J. Hansen, G. B. McManus, F. Not, H. do Rosario Gomes, L. F. Santoferrara, D. K. Stoecker, and U. Tillmann (2023). The Mixoplankton Database (MDB): Diversity of Photo-Phago-Trophic Plankton in Form, Function, and Distribution across the Global Ocean. *Journal of Eukaryotic Microbiology* n/a, e12972.

Mojica, K. D. A., J. Huisman, S. W. Wilhelm, and C. P. D. Brussaard (2016). Latitudinal Variation in Virus-Induced Mortality of Phytoplankton across the North Atlantic Ocean. *The ISME Journal* 10, 500–513.

Moon-van der Staay, S. Y., R. De Wachter, and D. Vaulot (2001). Oceanic 18S rDNA Sequences from Picoplankton Reveal Unsuspected Eukaryotic Diversity. *Nature* 409, 607–610.

Morel, F., J. Rueter, and N. Price (1991). Iron Nutrition of Phytoplankton and Its Possible Importance in the Ecology of Ocean Regions with High Nutrient and Low Biomass. *Oceanography* 4, 56–61.

Nodder, S. D., G. C. A. Duineveld, C. A. Pilditch, P. J. Sutton, P. K. Probert, M. S. S. Lavaleye, R. Witbaard, F. H. Chang, J. A. Hall, and K. M. Richardson (2007). Focusing of Phytodetritus Deposition beneath a Deep-Ocean Front, Chatham Rise, New Zealand. *Limnology and Oceanography* 52, 299–314.

Obiol, A., C. R. Giner, P. Sánchez, C. M. Duarte, S. G. Acinas, and R. Massana (2020). A Metagenomic Assessment of Microbial Eukaryotic Diversity in the Global Ocean. *Molecular Ecology Resources* 20, 718–731.

Oksanen, J. et al. (2022). *vegan: Community Ecology Package*. R package version 2.6-4.

Olofsson, M., O. Kourtchenko, E.-M. Zetsche, H. K. Marchant, M. J. Whitehouse, A. Godhe, and H. Ploug (2019). High Single-Cell Diversity in Carbon and Nitrogen Assimilations by a Chain-Forming Diatom across a Century. *Environmental Microbiology* 21, 142–151.

Ong, D. R. Y., A. Gutiérrez-Rodríguez, L. Garczarek, D. Marie, and A. Lopes dos Santos (2023). Nested PCR Approach for *petB* Gene Metabarcoding of Marine *Synechococcus* Populations. *Microbiology Spectrum* 0, e04086–22.

Pasciak, W. J. and J. Gavis (1974). Transport Limitation of Nutrient Uptake in Phytoplankton. *Limnology and Oceanography* 19, 881–888.

Peterson, B. J. (1980). Aquatic Primary Productivity and the $^{14}$C-$CO_2$ Method: A History of the Productivity Problem. *Annual Review of Ecology and Systematics* 11, 359–385.

Piredda, R., M. P. Tomasino, A. M. D'Erchia, C. Manzari, G. Pesole, M. Montresor, W. H. C. F. Kooistra, D. Sarno, and A. Zingone (2017). Diversity and Temporal Patterns of Planktonic Protist Assemblages at a Mediterranean Long Term Ecological Research Site. *FEMS Microbiology Ecology* 93, fiw200.

Pittera, J., F. Humily, M. Thorel, D. Grulois, L. Garczarek, and C. Six (2014). Connecting Thermal Physiology and Latitudinal Niche Partitioning in Marine *Synechococcus*. *ISME Journal* 8, 1221–1236.

Raven, J. A. (1998). The Twelfth Tansley Lecture. Small Is Beautiful: The Picophytoplankton. *Functional Ecology* 12, 503–513.

Rigual-Hernández, A. S., T. W. Trull, J. A. Flores, S. D. Nodder, R. Eriksen, D. M. Davies, G. M. Hallegraeff, F. J. Sierro, S. M. Patil, A. Cortina, A. M. Ballegeer, L. C. Northcote, F. Abrantes, and M. M. Rufino (2020). Full Annual Monitoring of Subantarctic *Emiliania Huxleyi* Populations Reveals Highly Calcified Morphotypes in High-$CO_2$ Winter Conditions. *Scientific Reports* 10, 2594.

Rii, Y., D. Karl, and M. Church (2016a). Temporal and Vertical Variability in Picophytoplankton Primary Productivity in the North Pacific Subtropical Gyre. *Marine Ecology Progress Series* 562, 1–18.

Rii, Y. M., S. Duhamel, R. R. Bidigare, D. M. Karl, D. J. Repeta, and M. J. Church (2016b). Diversity and Productivity of Photosynthetic Picoeukaryotes in Biogeochemically Distinct Regions of the South East Pacific Ocean. *Limnology and Oceanography* 61, 806–824.

Rose, J. M. and D. A. Caron (2007). Does Low Temperature Constrain the Growth Rates of Heterotrophic Protists? Evidence and Implications for Algal Blooms in Cold Waters. *Limnology and Oceanography* 52, 886–895.

RStudio Team (2021). *RStudio: Integrated Development Environment for R*. RStudio, PBC. Boston, MA.

Sabine, C. L., R. A. Feely, N. Gruber, R. M. Key, K. Lee, J. L. Bullister, R. Wanninkhof, C. S. Wong, D. W. R. Wallace, B. Tilbrook, F. J. Millero, T.-H. Peng, A. Kozyr, T. Ono, and A. F. Rios (2004). The Oceanic Sink for Anthropogenic CO2. *Science* 305, 367–371.

Safi, K. A. and J. A. Hall (1999). Mixotrophic and Heterotrophic Nanoflagellate Grazing in the Convergence Zone East of New Zealand. *Aquatic Microbial Ecology* 20, 83–93.

Schneider, L., K. Anestis, J. Mansour, A. Anschütz, N. Gypens, P. Hansen, U. John, K. Klemm, J. Martin, N. Medic, F. Not, and W. Stolte (2020). A Dataset on Trophic Modes of Aquatic Protists. *Biodiversity Data Journal* 8, e56648.

Selph, K. E. (2021). Enumeration of Marine Microbial Organisms by Flow Cytometry Using Near-UV Excitation of Hoechst 34580-Stained DNA. *Limnology and Oceanography: Methods* 19, 692–701.

Shi, X. L., D. Marie, L. Jardillier, D. J. Scanlan, and D. Vaulot (2009). Groups without Cultured Representatives Dominate Eukaryotic Picophytoplankton in the Oligotrophic South East Pacific Ocean. *PLoS One* 4, e7657.

Simmons, M. P., S. Sudek, A. Monier, A. J. Limardo, V. Jimenez, C. R. Perle, V. A. Elrod, J. T. Pennington, and A. Z. Worden (2016). Abundance and Biogeography of Picoprasinophyte Ecotypes and Other Phytoplankton in the Eastern North Pacific Ocean. *Applied and Environmental Microbiology* 82, 1693–1705.

Sohm, J. A., N. A. Ahlgren, Z. J. Thomson, C. Williams, J. W. Moffett, M. A. Saito, E. A. Webb, and G. Rocap (2016). Co-Occurring *Synechococcus* Ecotypes Occupy Four Major Oceanic Regimes Defined by Temperature, Macronutrients and Iron. *The ISME Journal* 10, 333–345.

Sommer, U., E. Charalampous, S. Genitsaris, and M. Moustaka-Gouni (2017). Benefits, Costs and Taxonomic Distribution of Marine Phytoplankton Body Size. *Journal of Plankton Research* 39, 494–508.

Sow, S. L. S., T. W. Trull, and L. Bodrossy (2020). Oceanographic Fronts Shape Phaeocystis Assemblages: A High-Resolution 18S rRNA Gene Survey From the Ice-Edge to the Equator of the South Pacific. *Frontiers in Microbiology* 11.

Stoecker, D. K. (1999). Mixotrophy among Dinoflagellates. *Journal of Eukaryotic Microbiology* 46, 397–401.

Stoecker, D. K., P. J. Hansen, D. A. Caron, and A. Mitra (2017). Mixotrophy in the Marine Plankton. *Annual Review of Marine Science* 9, 311–335.

Strzepek, R. F., M. T. Maldonado, J. L. Higgins, J. Hall, K. Safi, S. W. Wilhelm, and P. W. Boyd (2005). Spinning the "Ferrous Wheel": The Importance of the Microbial Community in an Iron Budget during the FeCycle Experiment. *Global Biogeochemical Cycles* 19.

Strzepek, R. F., M. T. Maldonado, K. A. Hunter, R. D. Frew, and P. W. Boyd (2011). Adaptive Strategies by Southern Ocean Phytoplankton to Lessen Iron Limitation: Uptake of Organically Complexed Iron and Reduced Cellular Iron Requirements. *Limnology and Oceanography* 56, 1983–2002.

Stukel, M. R., M. Décima, K. E. Selph, and A. Gutiérrez-Rodríguez (2021). Size-Specific Grazing and Competitive Interactions between Large Salps and Protistan Grazers. *Limnology and Oceanography* 66, 2521–2534.

Stukel, M. R., M. R. Landry, and K. E. Selph (2011). Nanoplankton Mixotrophy in the Eastern Equatorial Pacific. *Deep Sea Research Part II: Topical Studies in Oceanography* 58, 378–386.

Sutton, P. (2001). Detailed Structure of the Subtropical Front over Chatham Rise, East of New Zealand. *Journal of Geophysical Research: Oceans* 106, 31045–31056.

Thiele, S., C. Wolf, I. K. Schulz, P. Assmy, K. Metfies, and B. M. Fuchs (2014). Stable Composition of the Nano- and Picoplankton Community during the Ocean Iron Fertilization Experiment LOHAFEX. *PLOS ONE* 9, e113244.

Vaulot, D., W. Eikrem, M. Viprey, and H. Moreau (2008). The Diversity of Small Eukaryotic Phytoplankton ($\leq$3 $\mu$m) in Marine Ecosystems. *FEMS Microbiology Reviews* 32, 795–820.

Vihtakari, M. (2022). *ggOceanMaps: Plot Data on Oceanographic Maps using 'ggplot2'*. R package version 1.2.6.

Villiot, N., A. E. Maas, A. J. Poulton, and L. Blanco-Bercial (2023). Organic and Inorganic Nutrients Modulate Taxonomic Diversity and Trophic Strategies of Small Eukaryotes in Oligotrophic Oceans. *FEMS Microbes* 4, xtac029.

Ward, B. A., S. Dutkiewicz, A. D. Barton, and M. J. Follows (2011). Biophysical Aspects of Resource Acquisition and Competition in Algal Mixotrophs. *The American Naturalist* 178, 98–112.

Wickham, H. (2016). *ggplot2: Elegant Graphics for Data Analysis.*

Xia, X., S. Cheung, H. Endo, K. Suzuki, and H. Liu (2019). Latitudinal and Vertical Variation of *Synechococcus* Assemblage Composition Along 170ř W Transect From the South Pacific to the Arctic Ocean. *Microbial Ecology* 77, 333–342.

Zentara, S. J. and D. Kamykowski (1981). Geographic Variations in the Relationship between Silicic Acid and Nitrate in the South Pacific Ocean. *Deep Sea Research Part A. Oceanographic Research Papers* 28, 455–465.

Zhu, F., R. Massana, F. Not, D. Marie, and D. Vaulot (2005). Mapping of Picoeucaryotes in Marine Ecosystems with Quantitative PCR of the 18S rRNA Gene. *FEMS Microbiology Ecology* 52, 79–92.

Zhu, Z., K. Xu, F. Fu, J. L. Spackeen, D. A. Bronk, and D. A. Hutchins (2016). A Comparative Study of Iron and Temperature Interactive Effects on Diatoms and *Phaeocystis Antarctica* from the Ross Sea, Antarctica. *Marine Ecology Progress Series* 550, 39–51.

Zubkov, M. V. (2014). Faster Growth of the Major Prokaryotic versus Eukaryotic $CO_2$ Fixers in the Oligotrophic Ocean. *Nature Communications* 5, 3776.

Zubkov, M. V. and G. A. Tarran (2008). High Bacterivory by the Smallest Phytoplankton in the North Atlantic Ocean. *Nature* 455, 224–226.

Zwirglmaier, K., L. Jardillier, M. Ostrowski, S. Mazard, L. Garczarek, D. Vaulot, F. Not, R. Massana, O. Ulloa, and D. J. Scanlan (2008). Global Phylogeography of Marine *Synechococcus* and *Prochlorococcus* Reveals a Distinct Partitioning of Lineages among Oceanic Biomes. *Environmental Microbiology* 10, 147–161.

## Acknowledgements

We acknowledge the crew of RV *Tangaroa* for their efforts in facilitating the sampling throughout the TAN1810 voyage. We thank Daniel Vaulot (CNRS) for providing the equation to calculate group-specific carbon fixation rate and feedback on data processing. We are grateful to Jaret Bilewitch and Debbie Hulston (National Institute of Water and Atmospheric Research, New Zealand) for their laboratory work on the DNA extraction of filtered seawater samples and Debbie Hulston for coordinating the logistics of transporting the DNA extracted samples from New Zealand to Singapore. We thank Priscilla Gourvil for coordinating the logistics of transporting the sorted samples from France to Singapore. We thank Molly A. Moynihan (Marine Biological Laboratory) for laboratory assistance and guidance, as well as coordinating the logistics of Illumina sequencing. We thank Clarence Sim Wei Hung (Nanyang Technological University, Singapore) for providing the adapted trophic assignment database from Schneider et al. (2020), as well as laboratory assistance. We are grateful to Eleanor Slade and Ong Xin Rui (Nanyang Technological University, Singapore) for providing invaluable guidance on statistical analysis.

ALS and DO were supported by the Singapore Ministry of Education, Academic Research Fund Tier 1 (RG26/19). AGR was supported by NIWA via the New Zealand Ministry of Business, Innovation and Employments Strategic Science Investment Funding to the National Coasts Ocean Centre. KES was supported by NSF award #OCE-1756610.


## Availability of data and materials.

Source code (all sequence processing and analysis scripts) for this paper is available on Github (https://github.com/deniseong/TAN1810_C14). All unprocessed sequencing data have been deposited in NCBI Sequence Read Archive (*petB* (filtered and sorted samples)—PRJNA885274, 18SV4 (filtered samples)—PRJNA670061 and PRJNA1033349 (Table S4), 18SV4 (sorted samples)—PRJNA1033349). Raw data files from flow cytometry sorting are available on http://flowrepository.org/experiments/1773 (Repository ID: FR-FCM-Z5P8) and metadata for data files are available on https://github.com/deniseong/marine-Synechococcus-metaB.

# Author contributions statement

ALS, AG, KS have contributed to conception and designed. ALS, AG, KS, KES, DO have processed the samples and produced data. DO, AG, ALS, MS, KS have analysed and interpreted the data. DO and ALS have drafted the manuscript. All authors have revised and approved the final manuscript.

# Additional information

**Competing interests** The authors declare no competing financial interests.

# List of Tables


Table 1 **Cell-specific carbon fixation rates, group-specific productivity, cell abundance and carbon-fixation-based growth rates (mean ± SD) for *Synechococcus* (Syn), Picoeukaryotes (Pico) and Nanoeukaryotes (Nano) at each cycle**. Group-specific productivity was obtained by multiplying cell-specific rates by *Synechococcus*, picoeukaryotes and nanoeukaryotes cell abundances. Number of samples for each cycle and group are stated in brackets beside cell-specific carbon fixation values. . . . . 43

Table S1 Depths (m) sampled in the water column for various measurements at each cycle. Primary production refers to small phytoplankton cell-specific and net production (both standard and small volume). (*) depths in bold represent those used for small phytoplankton cell-specific and small volume net primary production experiments . . . . . 54

Table S2 Date, location and depth [at surface (SUR) and deep chlorophyll maximum (DCM)] of the samples used for $^{14}$C-bicarbonate incorporation measurements, as well as the number of cells sorted for each phytoplankton group (*Synechococcus,* picoeukaryotes and nanoeuaryotes) after $^{14}$C-bicarbonate incubation for 24 hours. . . . . 55

Table S3 Date, location and depth, at surface (SUR) and deep chlorophyll maximum (DCM), of the samples used for DNA sequencing after flow cytometry sorting, as well as the number of cells sorted for each phytoplankton group (*Synechococcus*, picoeukaryotes and nanoeuaryotes). Vial letters represent: i, initial water sample; A-C, light incubations; D, dark incubations. . . . . 57

Table S4 Date, location and depth, at surface (SUR) and deep chlorophyll maximum (DCM), of the filtered seawater samples amplified with the *petB* and V4 region of the 18S rRNA marker gene for *Synechococcus* and eukaryote populations. Sequences are deposited on NCBI BioProject with the specified accession number. . . . . 61

Table S5 Estimated marginal means (EMM) with 95% CI (in square brackets) of liner models with phytoplankton population and/or water mass as explanatory variables and cell-specific carbon fixation rate, group-specific productivity or growth rates as a response variable. . . 61

Table S6 Number of samples (n) and statistical results, with depth (surface or deep chlorophyll maximum) and water mass (subtropical or subantarctic cycles) as explanatory variables for cell-specific carbon fixation rate, group-specific productivity, growth rate and cell diameter of each phytoplankton group. . . . . 62

Table S7 Alpha diversity indices (Shannon and Simpson) and number of ASVs (mean ± standard deviation), as well as number of samples (n) from flow cytometry sorted samples of photosynthetic *Synechococcus*, picoeukaryote and nanoeukaryote populations in subtropical (ST) and subantarctic (SA) cycles. The taxonomic diversity was obtained through metabarcoding of the *petB* gene and V4 region of the 18S rRNA gene from *Synechococcus* and eukaryotic phytoplankton populations, respectively. . . . . 62

Table S8 The percentage of reads, presented as median and interquartile range (in brackets), of *Synechococcus* for each subclade in each cycle, obtained from filtered and sorted samples. The rows are arranged in descending order according to the median percentage of reads of each subclade in sorted samples. . . . . 63

Table S9 The percentage of reads, presented as median and interquartile range (in brackets), of photosynthetic picoeukaryotes for each class in each cycle, obtained from filtered and sorted samples. To obtain the relative abundance of photosynthetic picoeukaryotes from filtered samples, we filtered for the same ASVs present in the sorted picoeukaryote samples. Dinophyceae and *Emiliania huxleyi* were removed before plotting the composition of picoeukaryotes as these taxa likely belong to larger size fractions and would obscure the composition of other taxa. The rows are arranged in descending order according to the median percentage of reads of each class in sorted samples. . . . . 63

Table S10 The percentage of reads, presented as median and interquartile range (in brackets), of photosynthetic nanoeukaryotes for each class in each cycle, obtained from filtered and sorted samples. To obtain the relative abundance of photosynthetic nanoeukaryotes from filtered samples, we filtered for the same ASVs present in the sorted nanoeukaryote samples. Mamiellophyceae and Chloropicophyceae were removed before calculating the composition of nanoeukaryotes as these taxa likely belong to smaller size fractions and would obscure the composition of other taxa. The rows are arranged in descending order according to the median percentage of reads of each class in sorted samples. . . . . 64

Table S11 Range of cell-specific or single-cell carbon fixation rates (fgC cell$^{-1}$ h$^{-1}$) of *Synechococcus* (Syn), and small eukaryotes of three size groups: Pico 1 (average cell diameter <2 µm), Pico 2 (average cell diameter 2-3 µm) and Nano (average cell diameter >3 µm). Average cell size (Avg size; µm) of each population is indicated, if reported. Type indicates group or single-cell, whereby carbon fixation rates of populations are quantified through measuring the amount of carbon isotope in a known number of cells which are counted and sorted through flow cytometry (cell-specific), or in individual cells through NanoSIMS (single-cell), respectively. Accompanying phytoplankton community analysis is also indicated along with the methods used, whereby cells are obtained either through filtered seawater samples or flow cytometry (FCM) sorting of populations, followed by community analysis methods of fluorescence in-situ hybridisation (FISH) or metabarcoding of the V4 or V9 region of the 18S rRNA gene, chloroplast 16S rRNA gene or *petB* gene (only for *Synechococcus*). . . . . 65

# List of Figures

Figure 1 **Map of the study area and temperature-salinity plot of each experimental cycle.** A) Map of the study area at the Chatham Rise, east of Aotearoa-New Zealand. Sea surface temperature data (řC) was obtained from MODIS (NASA) and averaged over November 2018. Bathymetric lines (m) were obtained from Amante & Eakins (2009) and plotted with ggOceanMaps (Vihtakari 2022). Each point represents one $^{14}$C incubation experiment within an experimental cycle in subtropical (ST) and subantarctic (SA) waters. B) Temperature-salinity plot of each experimental cycle obtained from downcast CTD measurements from 0 to 150 m depth. . . . . 44

Figure 2 **Depth-integrated Chlorophyll *a* (Chl *a*) concentration and net primary production (NPP) of the euphotic zone of each experimental cycle.** A) Mean depth-integrated chl *a* concentration with proportion of size fractionated Chl *a*. Error bars represent standard deviation. B) Mean community net primary production with 95% confidence intervals. . . . . 45

Figure 3 **Phytoplankton productivity and carbon-based growth rates among *Synechococcus* (Syn), picoeukaryotes (Pico) and nanoeukaryotes (Nano) in subtropical (ST) and subantarctic (SA) water masses.** (A) Cell-specific carbon fixation rate (fgC cell$^{-1}$ h$^{-1}$), (B) group-specific productivity (mgC m$^{-3}$ day$^{-1}$) and (C) growth rate (day$^{-1}$). The violin plot shows the distribution of individual measurements, and the point-range plot represents the estimated marginal mean (EMM; dot) and 95% CI (line) of the model. There was no significant difference in group-specific productivity between water masses, therefore EMM and CI presented in (B) represents population. . . . . 46

Figure 4 **Non-metric multidimensional scaling (NMDS) of flow cytometry sorted A) *Synechococcus pet*B community and B) photosynthetic picoeukaryote and nanoeukaryote 18S rRNA community.** Each point corresponds to one sample. Samples are coloured by cycle and shapes denote *Synechococcus* (Syn), picoeukaryotes (Pico) and nanoeukaryotes (Nano). . . . . 47

Figure 5 **Heatmap showing the median relative abundance (%) of reads in each cycle at log scale for flow cytometry sorted populations, only including taxa that have a median relative abundance of more than 5% in at least one cycle.** Picoeukaryotes at order (A) and species (B) level, Nanoeukaryotes at order level (C) and *Synechococcus* at subclade level (D). Samples are ordered from left to right across a spatial gradient, from subtropical (ST) to subantarctic (SA) cycles. Taxa are grouped by class for eukaryotes: Mamiellophyceae (Mam), Prymnesiophyceae (Prym), Pelagophyceae (Pel), Chrysophyceae (Chry), Bacillariophyta (Bac), Cryptophyceae (Cryp), Dinophyceae (Dino) and Haptophyta Clade HAP3 (HAP3). *Synechococcus* is grouped by clades I and IV. . . . 48

Figure 6 **Range of cell-specific/single-cell phytoplankton productivity rates (fgC cell$^{-1}$ h$^{-1}$) from previous measurements compared to this study.** Rate measurements are obtained by distinguishing phytoplankton populations via flow cytometry cell sorting or hybridisation to measure cell-specific or single-cell rates. Phytoplankton populations include *Synechococcus* and small eukaryotes of three size groups: Pico 1 (average cell diameter <2 µm), Pico 2 (average cell diameter 2-3 µm) and Nano (average cell diameter >3 µm) following definitions of Vaulot et al. (2008). Colours indicate water mass where measurements were taken. Outliers of this study are indicated with points. Full summary of average cell size, experimental design and sampling location can be found in Table S11. 49

Figure S1 Phytoplankton cell abundances for *Synechococcus* (Syn), picoeukaryotes (Pico) and nanoeukaryotes (Nano) at surface(SUR) and deep chlorophyll maximum (DCM), represented by shapes. . . . . 67

Figure S2 Cell-specific carbon fixation rate for *Synechococcus* (Syn), picoeukaryotes (Pico) and nanoeukaryotes (Nano). Each experiment represents one incubation with radioactively labelled $^{14}$C-bicarbonate conducted in triplicates at two depths, surface(SUR) and deep chlorophyll maximum (DCM), represented by shapes. . . . . 68

Figure S3 Group-specific productivity for *Synechococcus* (Syn), picoeukaryotes (Pico) and nanoeukaryotes (Nano), obtained by multiplying the carbon fixation rate with cell abundance. Each experiment is one incubation with radioactively labelled $^{14}$C-bicarbonate conducted in triplicates at two depths of surface (SUR) and deep chlorophyll maximum (DCM), represented by shapes. . . . . 69

Figure S4 Carbon-based phytoplankton growth rate of *Synechococcus* (Syn), picoeukaryotes (Pico) and nanoeukaryotes (Nano) for each cycle. ST and SA refers to subtropical and subantarctic water masses, respectively. . . . . 70
Figure S5 Depth profiles of sampled water masses for physical measurements of A) temperature, B) salinity and C) PAR nitrate, nutrient measurements of D) ammonia, E) nitrate, F) phosphorus and G) silicate, and phytoplankton cell abundances of H) *Synechococcus*, I) Picoeukaryotes and J) Nanoeukaryotes of each cycle. Smoothing curveis obtained by LOESS (locally estimated scatterplot smoothing) of all measurements within each cycle. A to C profiles were obtained from downcast CTD measurements. . . . . 71
Figure S6 Proportion of size-fractionated chlorophyll *a* for each cycle. . . . . 72
Figure S7 Heatmap showing the median relative abundance (%) of reads in each cycle for flow cytometry sorted nanoeukaryotes at species levels, only including taxa that have a median relative abundance of more than 5% in at least one cycle. Samples are ordered from left to right across a spatial gradient, from subtropical (ST) to subantarctic (SA) cycles. Taxa are grouped by class, followed by order. . . . . 73
Figure S8 Net primary productivity (NPP) measurements from standard volume (320 mL) and small volume (7.4 mL) incubations, indicated by colour, at surface (SUR) and DCM (deep chlorophyll maximum). Each experiment (2-11, accompanied by cell-specific carbon fixation measurements) or station (339 and 353 in SA2, without corresponding group-specific carbon fixation measurements) is one incubation conducted in triplicates. Each point represents one replicate, and each line indicates the average NPP of standard or small volume incubation. . . . . 74
Figure S9 *Synechococcus* taxonomic composition at subclade level from flow cytometry sorted samples before incubation (i), and after 24 h incubation in light (triplicates of A, B, C) and dark (D). Samples were grouped by depth sampled of surface (SUR) and deep chlorophyll maximum (DCM), and incubation experiment (1-11). Each incubation experiment was labelled as 'cycle'_'experiment', and ordered across a spatial gradient from subtropical (ST) to subantarctic (SA) cycles. Missing samples were either lost during incubation or could not be amplified. . . . . 75
Figure S10 Photosynthetic picoeukaryote taxonomic composition at class level from flow cytometry sorted samples before incubation (i), and after 24 h incubation in light (triplicates of A, B, C) and dark (D). Samples were grouped by depths sampled of surface (SUR) and deep chlorophyll maximum (DCM), and incubation experiment (1-11). Each incubation experiment was labelled as 'cycle'_'experiment', and ordered across a spatial gradient from subtropical (ST) to subantarctic (SA) cycles. Missing samples were either lost during incubation or could not be amplified. . . . . 76
Figure S11 Photosynthetic nanoeukaryote taxonomic composition at order level from flow cytometry sorted samples before incubation (i), and after 24 h incubation in light (triplicates of A, B, C) and dark (D). Samples were grouped by depth sampled of surface (SUR) and deep chlorophyll maximum (DCM), and incubation experiment (1-11). Each incubation experiment was labelled as 'cycle'_'experiment', and ordered across a spatial gradient from subtropical (ST) to subantarctic (SA) cycles. Missing samples were either lost during incubation or could not be amplified. . . . . 77

# Tables

**Table 1: Cell-specific carbon fixation rates, group-specific productivity, cell abundance and carbon-fixation-based growth rates (mean ± SD) for *Synechococcus* (Syn), Picoeukaryotes (Pico) and Nanoeukaryotes (Nano) at each cycle**. Group-specific productivity was obtained by multiplying cell-specific rates by *Synechococcus*, picoeukaryotes and nanoeukaryotes cell abundances. Number of samples for each cycle and group are stated in brackets beside cell-specific carbon fixation values.

| Group | ST1 | ST2 | SA-Sc | SA1 | SA2 |
|---|---|---|---|---|---|
| | Cell-specific $CO_2$ fixation (fgC cell$^{-1}$ h$^{-1}$) | | | | |
| Syn | 1.04 ± 0.99 (3) | 1.41 ± 0.30 (11) | 0.25 ± 0.14 (5) | 0.56 ± 0.27 (15) | 0.32 ± 0.09 (5) |
| Pico | 2.57 ± 3.32 (3) | 2.29 ± 0.73 (11) | 0.40 ± 0.21 (5) | 2.94 ± 2.80 (15) | 1.37 ± 0.79 (6) |
| Nano | 29.27 ± 12.60 (3) | 55.96 ± 22.98 (11) | 40.58 ± 5.66 (6) | 67.60 ± 37.28 (16) | 27.60 ± 7.72 (6) |
| | Cell abundance (Œ $10^3$ cells mL$^{-1}$) | | | | |
| Syn | 83.98 | 16.03 ± 4.79 | 31.87 ± 5.83 | 67.15 ± 21.69 | 42.80 ± 31.26 |
| Pico | 19.41 | 12.81 ± 5.09 | 24.36 ± 0.60 | 11.44 ± 2.10 | 6.25 ± 3.18 |
| Nano | 2.22 | 1.77 ± 0.84 | 1.43 ± 0.33 | 2.38 ± 0.30 | 1.16 ± 0.52 |
| | Group-specific productivity (mgC m$^{-3}$ day$^{-1}$) | | | | |
| Syn | 2.10 ± 1.99 | 0.55 ± 0.23 | 0.18 ± 0.08 | 0.89 ± 0.55 | 0.27 ± 0.12 |
| Pico | 1.20 ± 1.55 | 0.64 ± 0.23 | 0.23 ± 0.12 | 0.88 ± 0.97 | 0.15 ± 0.02 |
| Nano | 1.56 ± 0.67 | 2.64 ± 1.94 | 1.40 ± 0.40 | 3.97 ± 2.45 | 0.84 ± 0.55 |
| | C-based growth rate (day$^{-1}$) | | | | |
| Syn | 0.19 ± 0.18 | 0.29 ± 0.10 | 0.06 ± 0.03 | 0.11 ± 0.06 | 0.07 ± 0.02 |
| Pico | 0.29 ± 0.37 | 0.29 ± 0.10 | 0.07 ± 0.03 | 0.30 ± 0.29 | 0.17 ± 0.09 |
| Nano | 0.10 ± 0.04 | 0.33 ± 0.19 | 0.32 ± 0.12 | 0.34 ± 0.19 | 0.17 ± 0.03 |

# Figures

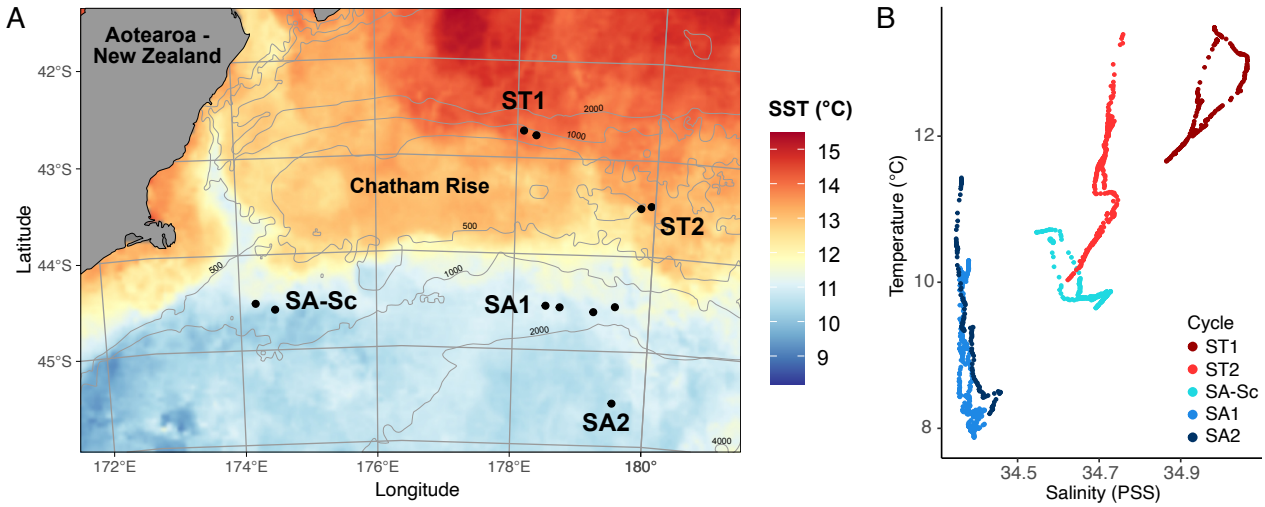


**Figure 1: Map of the study area and temperature-salinity plot of each experimental cycle.** A) Map of the study area at the Chatham Rise, east of Aotearoa-New Zealand. Sea surface temperature data (řC) was obtained from MODIS (NASA) and averaged over November 2018. Bathymetric lines (m) were obtained from Amante & Eakins (2009) and plotted with ggOceanMaps (Vihtakari 2022). Each point represents one $^{14}C$ incubation experiment within an experimental cycle in subtropical (ST) and subantarctic (SA) waters. B) Temperature-salinity plot of each experimental cycle obtained from downcast CTD measurements from 0 to 150 m depth.

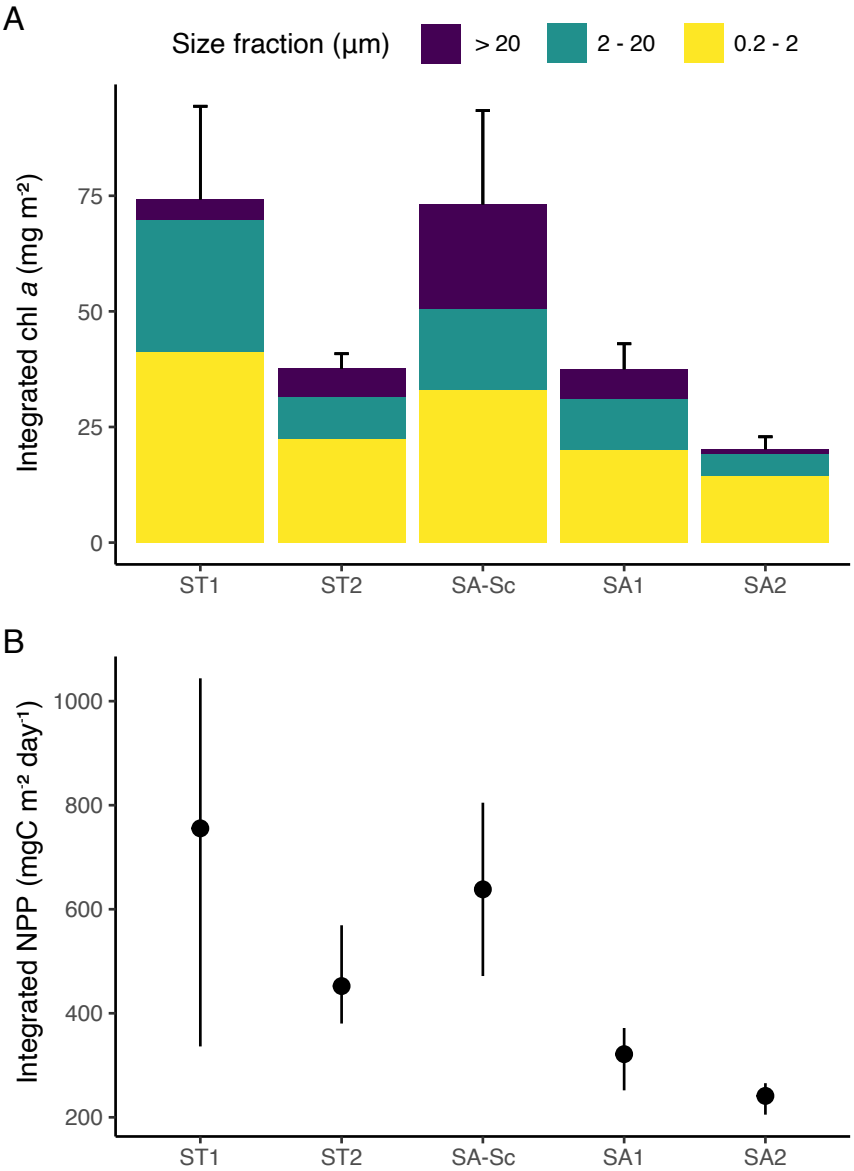


**Figure 2: Depth-integrated Chlorophyll *a* (Chl *a*) concentration and net primary production (NPP) of the euphotic zone of each experimental cycle.** A) Mean depth-integrated chl *a* concentration with proportion of size fractionated Chl *a*. Error bars represent standard deviation. B) Mean community net primary production with 95% confidence intervals.

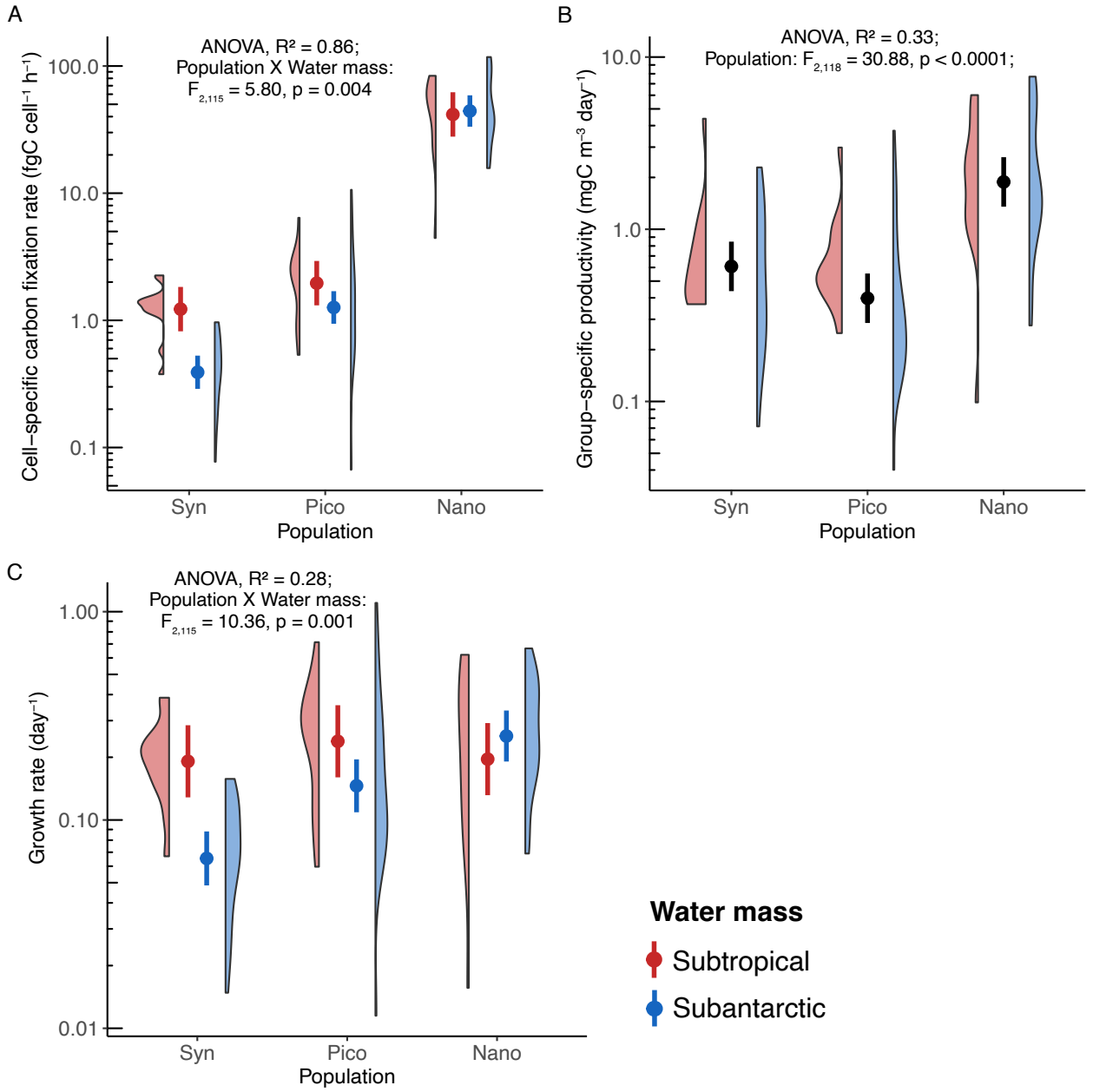


**Figure 3: Phytoplankton productivity and carbon-based growth rates among *Synechococcus* (Syn), picoeukaryotes (Pico) and nanoeukaryotes (Nano) in subtropical (ST) and subantarctic (SA) water masses.** (A) Cell-specific carbon fixation rate (fgC cell$^{-1}$ h$^{-1}$), (B) group-specific productivity (mgC m$^{-3}$ day$^{-1}$) and (C) growth rate (day$^{-1}$). The violin plot shows the distribution of individual measurements, and the point-range plot represents the estimated marginal mean (EMM; dot) and 95% CI (line) of the model. There was no significant difference in group-specific productivity between water masses, therefore EMM and CI presented in (B) represents population.

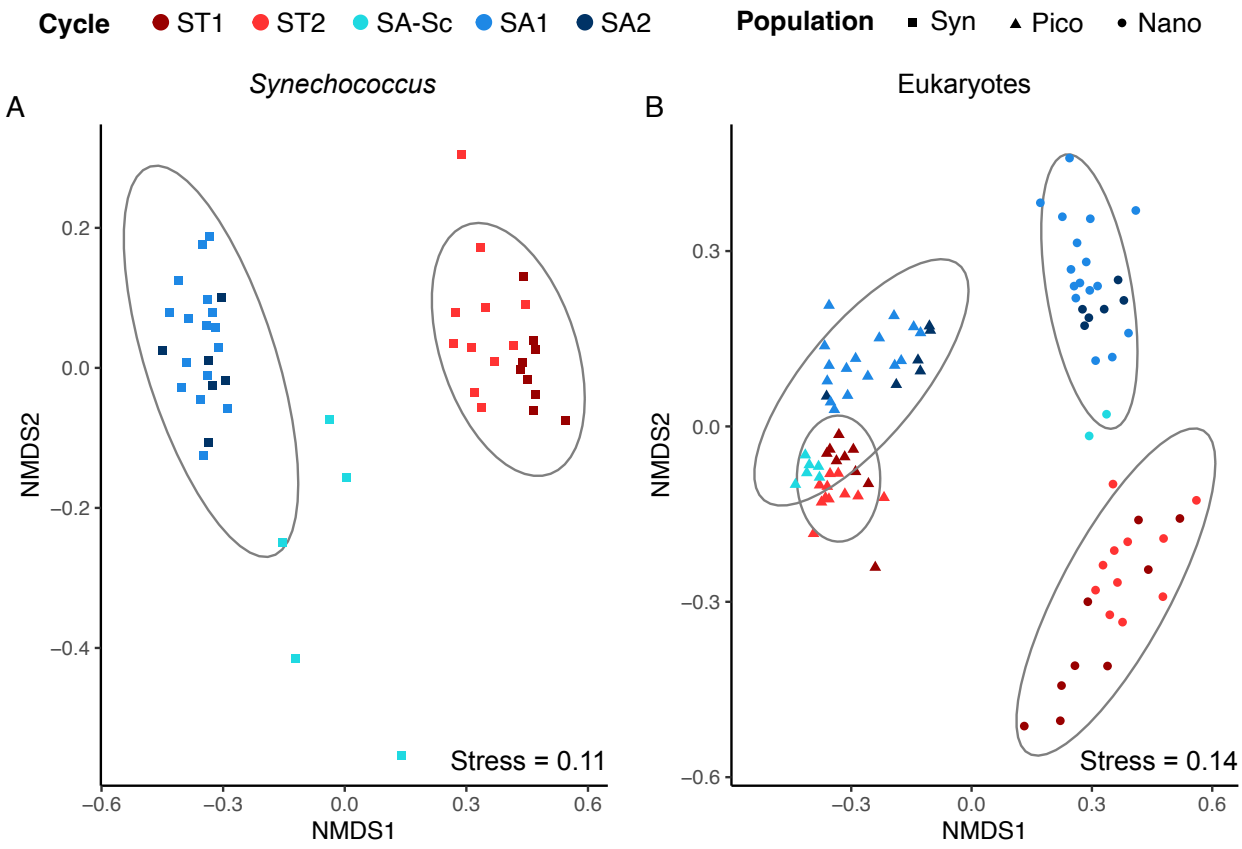


**Figure 4: Non-metric multidimensional scaling (NMDS) of flow cytometry sorted A) *Synechococcus pet*B community and B) photosynthetic picoeukaryote and nanoeukaryote 18S rRNA community.** Each point corresponds to one sample. Samples are coloured by cycle and shapes denote *Synechococcus* (Syn), picoeukaryotes (Pico) and nanoeukaryotes (Nano).

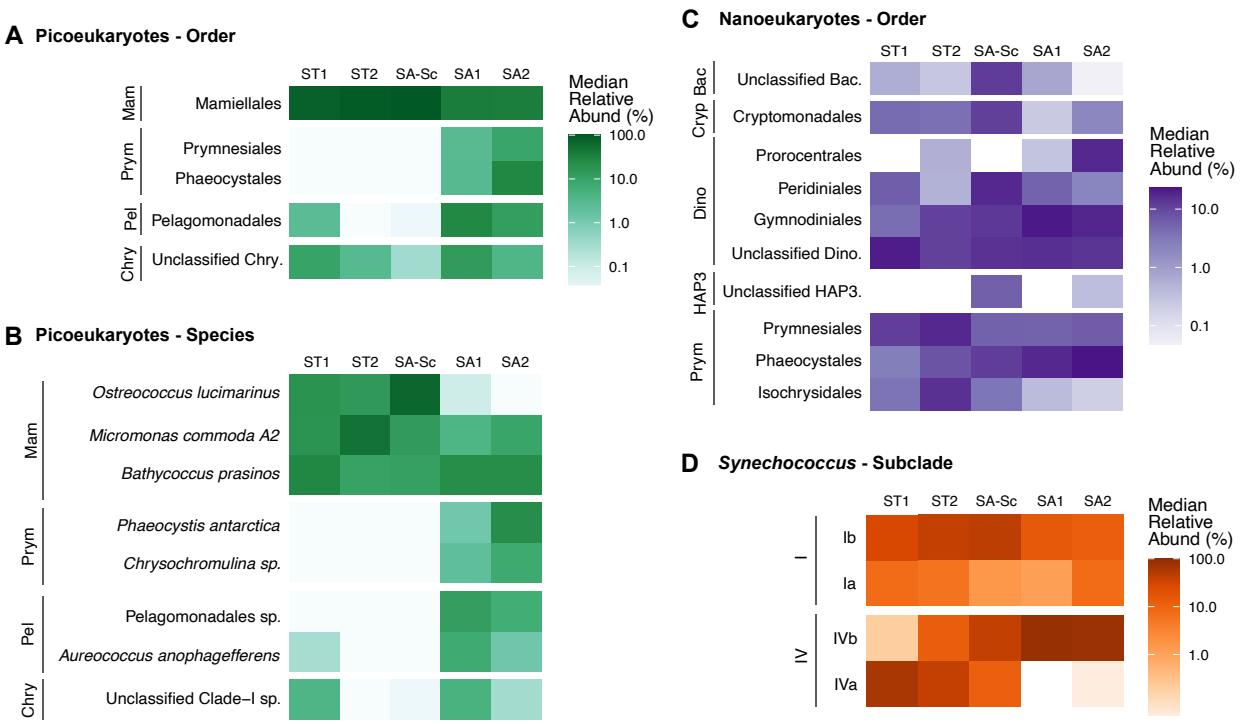


**Figure 5: Heatmap showing the median relative abundance (%) of reads in each cycle at log scale for flow cytometry sorted populations, only including taxa that have a median relative abundance of more than 5% in at least one cycle.** Picoeukaryotes at order (A) and species (B) level, Nanoeukaryotes at order level (C) and *Synechococcus* at subclade level (D). Samples are ordered from left to right across a spatial gradient, from subtropical (ST) to subantarctic (SA) cycles. Taxa are grouped by class for eukaryotes: Mamiellophyceae (Mam), Prymnesiophyceae (Prym), Pelagophyceae (Pel), Chrysophyceae (Chry), Bacillariophyta (Bac), Cryptophyceae (Cryp), Dinophyceae (Dino) and Haptophyta Clade HAP3 (HAP3). *Synechococcus* is grouped by clades I and IV.

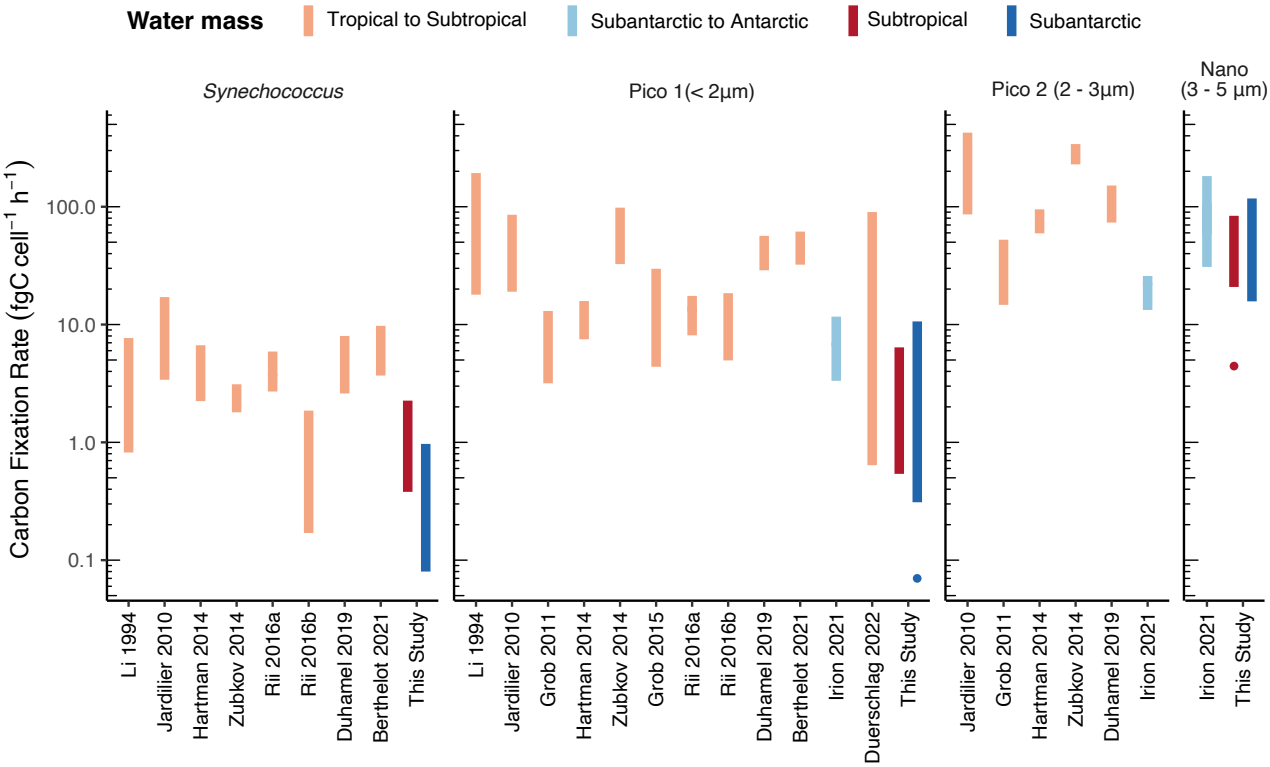


**Figure 6: Range of cell-specific/single-cell phytoplankton productivity rates (fgC cell$^{-1}$ h$^{-1}$) from previous measurements compared to this study.** Rate measurements are obtained by distinguishing phytoplankton populations via flow cytometry cell sorting or hybridisation to measure cell-specific or single-cell rates. Phytoplankton populations include *Synechococcus* and small eukaryotes of three size groups: Pico 1 (average cell diameter <2 µm), Pico 2 (average cell diameter 2-3 µm) and Nano (average cell diameter >3 µm) following definitions of Vaulot et al. (2008). Colours indicate water mass where measurements were taken. Outliers of this study are indicated with points. Full summary of average cell size, experimental design and sampling location can be found in Table S11.